Radant Analysis Studies

C. T. Tai and R. M. Kalafus

ABSTRACT

A review is given of the work performed on the loop-loaded radant panel, and its transmission properties. The recent work covered in detail herein deals with the transmission and polarization transformation properties of the crossed-dipole radant panel. A theoretical treatment is given based on knowledge of the element input impedance. The experimental program is described which yields information on transmission properties, polarization characteristics, beamwidth, bandwidth, sidelobe level, and patterns.

FOREWORD

This report was prepared by The University of Michigan under Contract No. AF 33(615)-2811, Task 416103, Project 4171. The work was administered under the direction of the Air Force Avionics Laboratory, Research and Technology Division, Air Force Systems Command: E. M. Turner, Technical Monitor, S. Pitts, Project Engineer.

This final technical report - Phase II, covers the work conducted from 1 March 1966 through 1 January 1967. The University of Michigan report number is 07300-2-F.

This report was submitted by the authors February 1967.

JOSEPH A. DOMBROWKI
Lt Colonel, USAF
Chief, Electronic Warfare Division

TABLE OF CONTENTS

		Page
	ABSTRACT	iii
	LIST OF ILLUSTRATIONS	vi
I	INTRODUCTION	1
	Summary of Interim Reports	1
II	CROSSED-POLARIZED RADANT PANEL	4
	2.1 Purpose and Summary	4
	2.2 Description of Radant Panel	4
III	THEORETICAL DISCUSSION OF SCATTERING BY A PERPENDICULAR DIPOLE PAIR LINKED BY A TRANSMISSION LINE	11
	3.1 Formulation of the Problem	11
	3.2 Optimum Conditions	15
	3.3 An Example	17
	3.4 Scattered Fields of Dipole Pair	19
IV	PROPERTIES OF A SINGLE DIPOLE ON A DIELECTRIC SHEET	22
	4.1 Dipole Impedance	22
	4.2 Critical Frequencies	22
	4.3 Power Transferred as a Function of Frequency	25
V	EXPERIMENTAL RESULTS OF A RADANT PANEL	32
	5.1 Patterns of the Horn-Radant Assembly	32
	5.2 Effects of Variation in Horn-Radant Spacing	46
	5.3 Polarization Characteristics	54
VI	CONCLUSIONS AND RECOMMENDATIONS FOR FUTURE WORK	59
	REFERENCES	60

LIST OF ILLUSTRATIONS

Figure — Page

2-1: Orientation of Dipole Arrays (only 9 dipole pairs shown for clarity). 5

2-2: Arrangement of Dipole Elements of Fiberglass Panel. 6

2-3: Radant Dipole Element. 8

2-4: Radant in Wooden Frame. 9

2-5: Radant Panel and Receiving Horn Geometry. 10

3-1: Perpendicular Dipoles Linked by a Pair of Transmission Lines 12

3-2: Equivalent Circuit of Dipole Pair 12

3-3: Graph for Determination of Critical Frequencies in Example Problem. 18

4-1: Dipole Impedance 23

4-2: Dipole Element and Balun 24

4-3: Dipole Impedance and Determination of Critical Frequency. 26

4-4: Calculated Directivity and Beamwidth of Dipole Element. 28

4-5: Effective Height of Dipole Element 29

4-6: Polarization Conversion Factor N 31

5-1: Block Diagram of Measurements 33

5-2a-v: Cross-Polarized Patterns of Horn-Radant Assembly, VVHH, 15 in. Spacing. 35-38

5-3a-v: Cross-Polarized Patterns of Horn-Radant Assembly, VHVH, 15 in. Spacing. 39-42

5-4: Transmission Coefficients, VVHX 44

5-5: Transmission Coefficients, VHVX 45

5-6a: Sidelobe Level, VHVH 47

5-6b: Beamwidth, VVHH 47

5-7a: Sidelobe Level, 48

5-7b: Beamwidth, VHVH 48

LIST OF ILLUSTRATIONS
(continued)

Figure Page

5-8a: Incident Pattern of Horn-Radant Assembly at 2.3 GHz, V--V, 15 in. Spacing. 49

5-8b: Like-Polarized Pattern of Radant Assembly at 2.3 GHz, VVHV, 15 in. Spacing. 49

5-8c: Like-Polarized Pattern of Radant Assembly at 2.3 GHz, VHVV, 15 in. Spacing. 49

5-9a: Incident Pattern of Horn-Radant Assembly at 2.4 GHz, V--V, 15 in. Spacing. 50

5-9b: Like-Polarized Pattern of Radant Assembly at 2.4 GHz, VVHV, 15 in. Spacing. 50

5-9c: Like-Polarized Pattern of Radant Assembly at 2.4 GHz, VHVV, 15 in. Spacing. 50

5-10a: Incident Pattern of Horn-Radant Assembly at 2.5 GHz, V--V, 15 in. Spacing. 51

5-10b: Like-Polarized Pattern of Radant Assembly at 2.5 GHz, VVHV, 15 in. Spacing. 51

5-10c: Like-Polarized Pattern of Radant Assembly at 2.5 GHz, VHVV, 15 in. Spacing. 51

5-11a-e: Cross-Polarized Pattern, VVHH, 3.6 GHz. 52

5-12a-d: Cross-Polarized Pattern, VHVH, 3.6 GHz. 53

5-13a: Inclination of Major Axis, XVHH. 55

5-13b: Axial Ratio, XVHH. 55

5-14a: Inclination of Major Axis, XHVH. 56

5-14b: Axial Ratio, XHVH. 56

5-15a-e: Polarization Pattern, XHVH, 15 in. Spacing. 57

I
INTRODUCTION

This report covers the research which has been done on "Radant Analysis Studies" from 30 April 1965 through 1 January 1967.

Except during the last period (1 September 1966 through 31 January 1967), the detailed studies have been presented in Interim Reports No. 1 to No. 4. (Report Nos. 7300-1-T through 7300-4-T), and the Final Report No. 7300-1-F (AFAL-TR-66-186) of the first phase. A summary of these reports are given below.

Summary of Interim Reports

Interim Report No. 1 (30 April through 31 July 1965) includes an analysis of the transmission of plane electromagnetic wave through an artificial anisotropic panel. The artificial dielectric under consideration consists of arrays of small conducting disks. The result of the analysis indicates that by properly adjusting the lattice parameters it is possible to change the transmission coefficient of the panel which cannot be accomplished by an isotropic panel. It is anticipated that a further study will be made in the coming year to extend the analysis contained in this report. The report also contains a preliminary theoretical investigation of the transmission characteristics of a finite panel excited by a line source. Physical optics approximation was used in the formulation. The result is compared with the experimental measurement which is also described in this report. A fairly good agreement is observed concerning the beamwidth of the resultant radiation pattern against the primary source spacing. In addition to the pattern measurement, the effect of the panel on a ferrite loaded slot antenna is also investigated. It was observed that the minimum VSWR of the slot antenna is relatively insensitive to the location of the panel. However, the resonant frequency does shift in the presence of the panel.

Interim Report No. 2 (31 July through 31 October 1965) contains a detailed experimental study of the characterisitics of a panel formed by rectangular loops. The panel is excited, respectively, by a ferrite-loaded slot antenna, a ridged horn,

and a half-wave dipole. The impedance of the antenna in the presence of the panel is measured. The resultant pattern of the antenna system is also recorded at several distinct frequencies. In general, the patterns are very dependent upon the spacing between the primary source and the panel. The report also contains a theoretical discussion of the scattering mechanism of two dipole linked by a pair of transmission lines. The theory takes into consideration the coupling between the two dipoles.

The work completed in the first year was compiled in the Final Report First Phase. In that report, the theoretical work, authored by M. Plonus, on the diffracted field due to a finite dielectric panel was presented in detail that includes a good amount of numerical calculation.

Interim Report No. 3 (1 February through 31 May 1966) contains an analysis of the scattered field of two crossed dipoles. It was predicted from the theoretical study that when the transmission line which links the two dipoles is matched to the antennas the scattered field due to the two dipoles would be of comparable strength. In order to meet the matching condition, an experimental study was undertaken to determine the input impedance of a dipole in the presence of a dielectric panel. It was observed that both the resonant frequency and the input impedance change considerably as compared to its free-space values.

Interim Report No. 4 (1 June through 31 August 1966) describes in detail the experimental set-up of the crossed-dipole panel.

Numerous patterns have been recorded in two principal planes to determine the transmission and cross-polarization effects of the panel.

The remaining sections of this final report present a theoretical interpretation of the experimental results which have been obtained during the final period of this contract (1 September 1966 through 31 January 1967).

According to this study, it appears that the transmission property of a panel

made of crossed-dipoles linked by transmission lines has been investigated quite thoroughly, both theoretically and experimentally. Within a properly chosen frequency band the panel is capable of converting linearly polarized field into an approximately circularly polarized field. The implication of this finding is discussed in the conclusion.

II

CROSSED-POLARIZED RADANT PANEL

2.1 Purpose and Summary

The purpose of this study is to determine to what extent a radant panel placed near a radiator can be used to transform polarization from linear to elliptical, or to rotate the direction of linear polarization so as to obtain a horizontal component from a vertically polarized radiator. The radant panel consists of two planar dipole arrays etched on thin fiberglass sheets, connected by two-wire transmission lines, and oriented perpendicularly to each other in polarization. Pyramidal horns were used as transmitting and receiving antennas.

The investigation showed the feasibility of attaining the desired polarization conversion over two narrow bands of frequencies with the particular structure chosen. The horizontal and vertical components are within 3 db of each other over approximately a 5 percent and 6 percent bandwidth. The scattered field of the vertical dipoles tends to cancel the vertically polarized incident wave at the receiving horn over the bands of operation. The antenna-to-panel spacing affects the overall level and the frequency dependence of the device, due to changes in input impedance at the receiving horn produced by the presence of the radant panel. At frequencies below the first band of operation the dipole elements are too small electrically to have any effect. Above the second resonance the spacing between elements becomes of the order of the wavelength and the sidelobe level becomes intolerable.

2.2 Description of Radant Panel

The radant panel consists of two sheets of 196 dipole each, imprinted on a 36-inch square, 1/16-inch fiberglass board, shown in Figs. 2-1 and 2-2. The two sheets are oriented parallel to each other but in such a way that each (vertical) dipole on one is connected by a two-wire transmission line one inch long to a (horizontal) dipole on the other. The transmission lines are made of AWG-20 wire

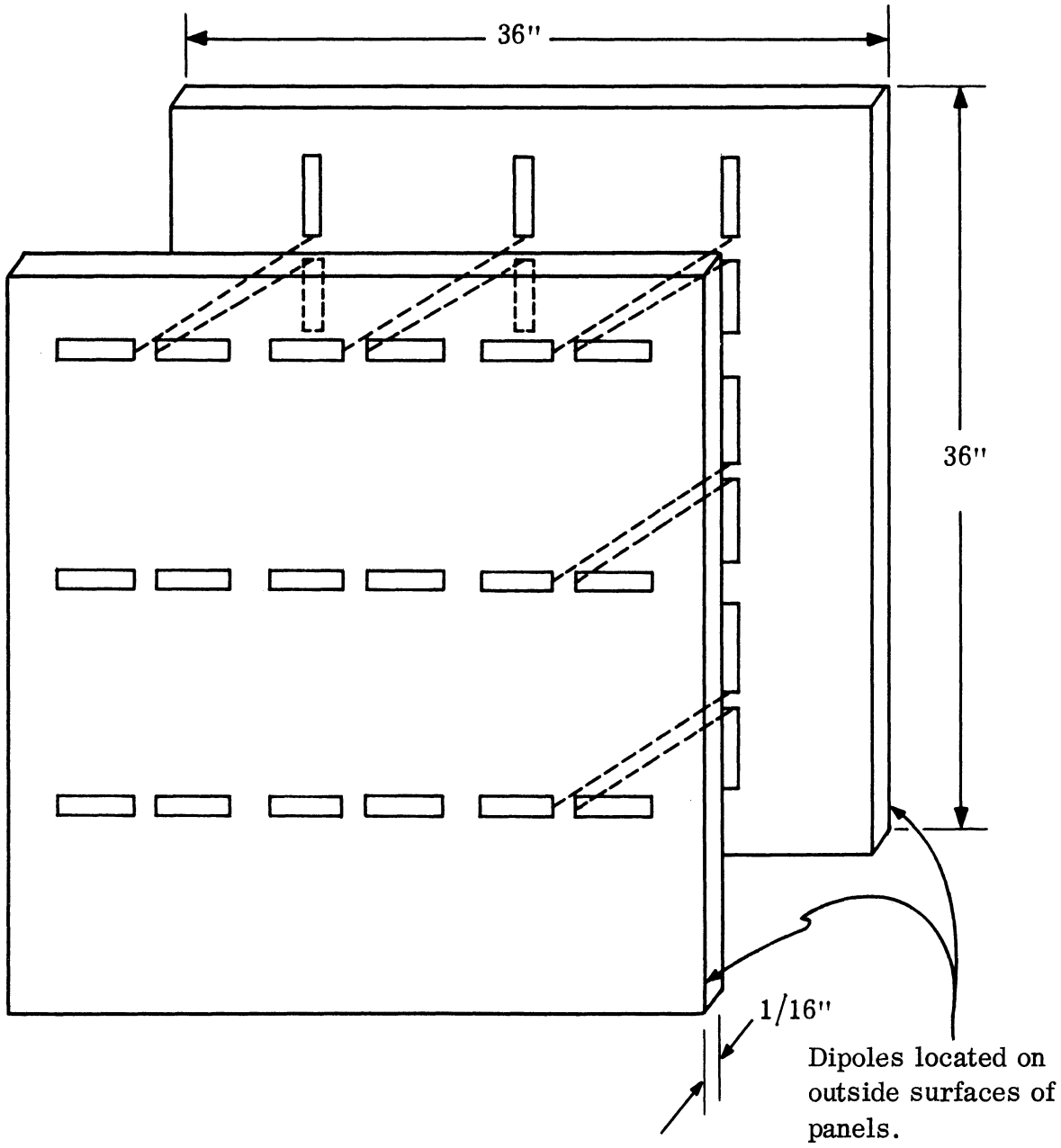

FIG. 2-1: ORIENTATION OF DIPOLE ARRAYS
(only 9 dipole pairs shown for clarity).

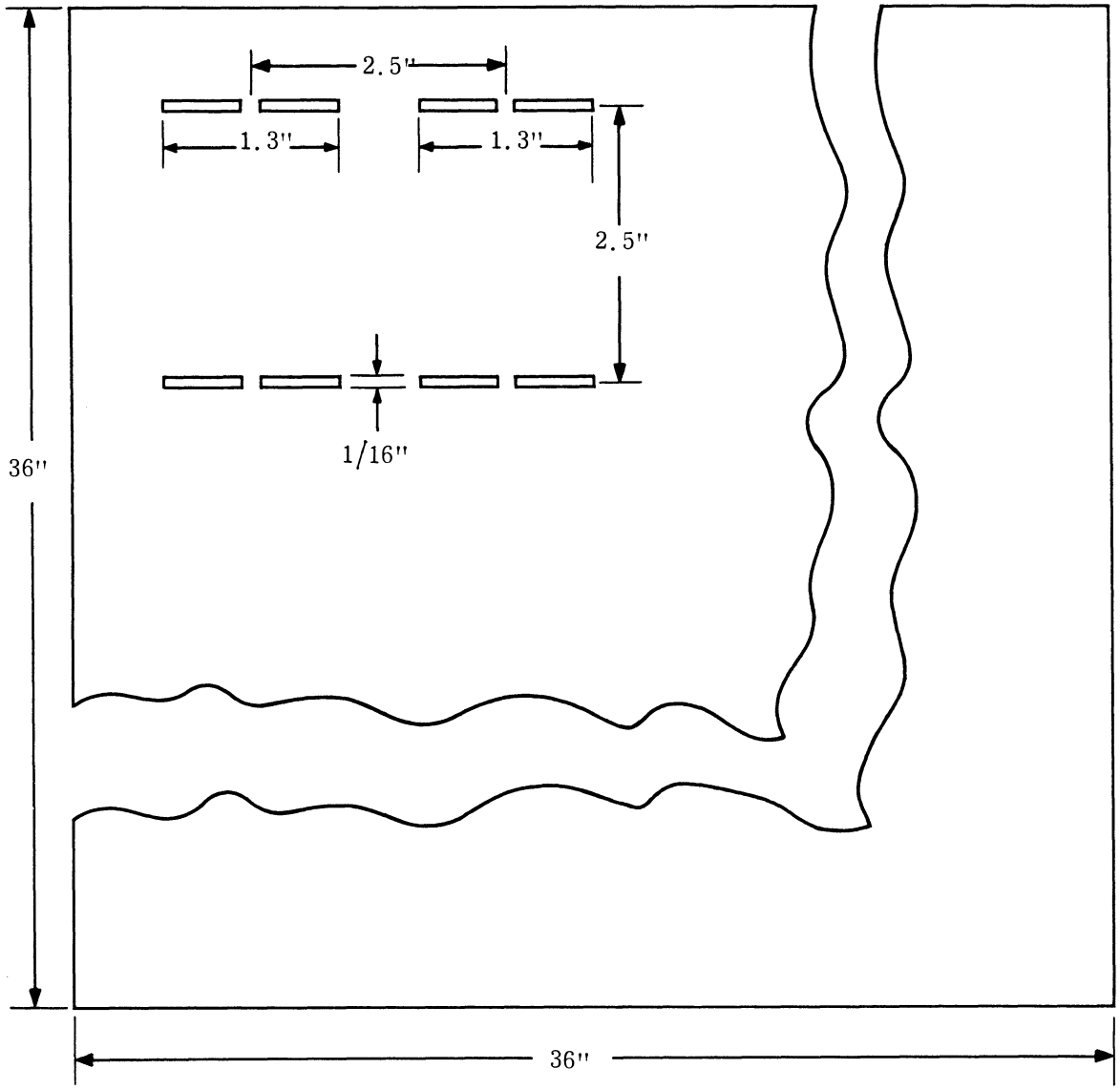
2.5"
1.3"
1.3"
2.5"
1/16"
36"
36"

separated by 0.06 inch, corresponding to an impedance of 160 ohms. Rather than twist the wires, the feed region of the dipoles was modified as shown in Fig. 2-3.

For strength, the radant is enclosed in a wooden frame (Fig. 2-4). This fits snugly into a vertical supporting rack, which is free to run forward and back along a track parallel to the line joining the transmitting and receiving antennas, as shown in Fig. 2-5. The track allows continuous adjustment of the spacing between radant and receiving antenna. The whole system is mounted on an antenna platform and can be rotated through the azimuth plane; that is, the angle ϕ of Fig. 2-5 can be varied continuously.

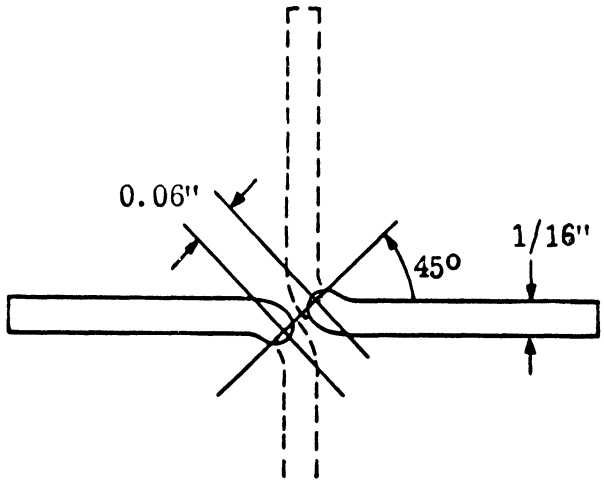

FIG. 2-3: RADANT DIPOLE ELEMENT

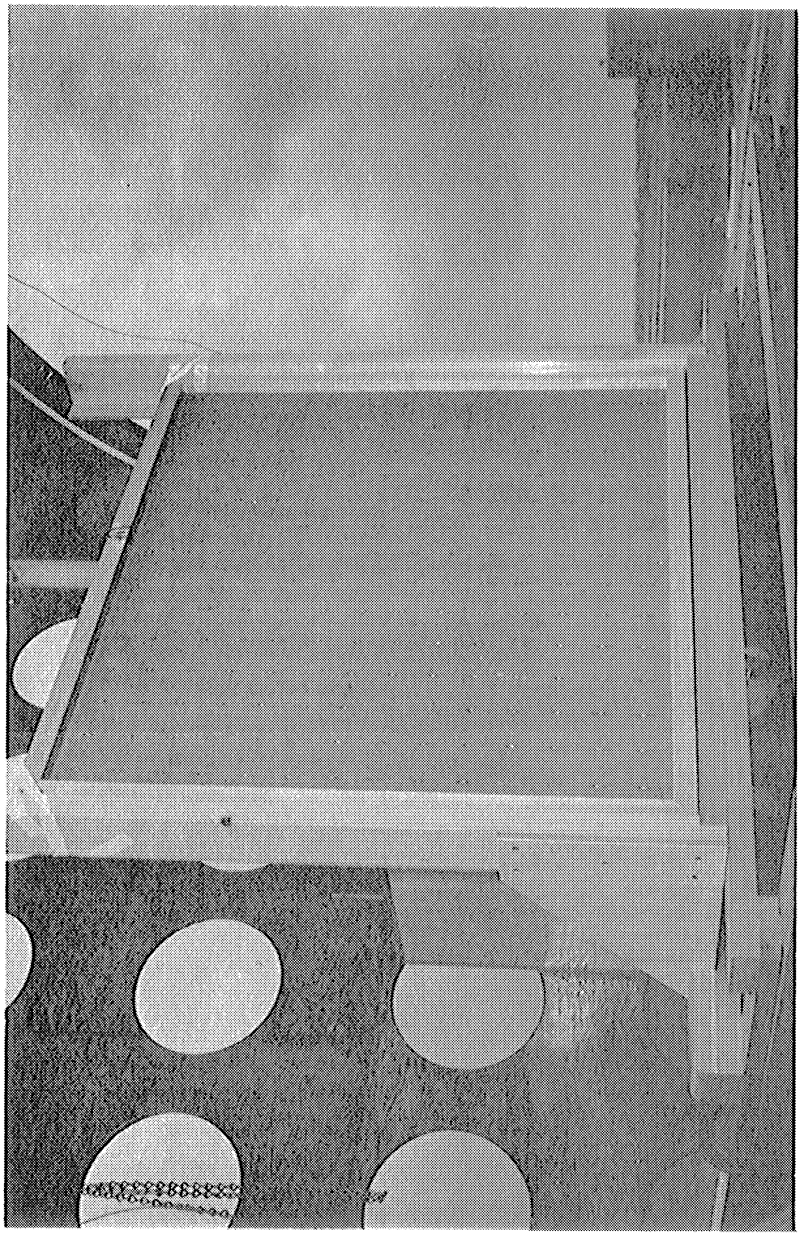

FIG 2-4: RADANT IN WOODEN FRAME

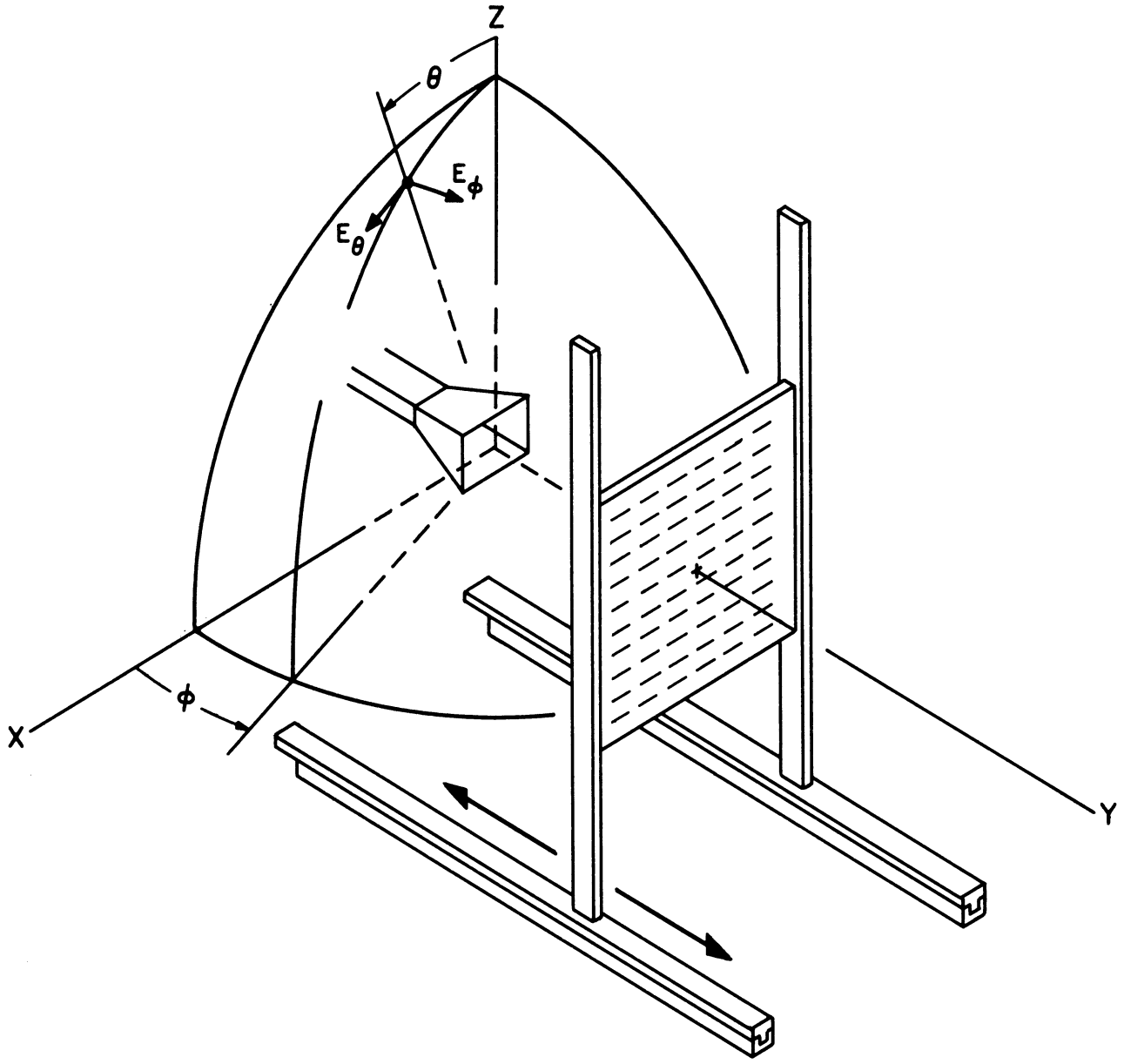

FIG. 2-5: RADANT PANEL AND RECEIVING HORN GEOMETRY

III

THEORETICAL DISCUSSION OF A SCATTERING BY A PERPENDICULAR DIPOLE PAIR LINKED BY A TRANSMISSION LINE

3.1 Formulation of the Problem

The problem under consideration is illustrated in Figs. 3-1 and 3-2.

Following the theory of receiving antennas, it can be shown that the short-circuit current induced at the terminals of antenna No. 1 is given by

$$I_1^{(s)} = Y_{11}\,\bar{h}_1 \cdot \bar{E}_1 \tag{3.1}$$

where

Y_{11} = self-admittance of antenna No. 1, defined in the presence of antenna No. 2

$\bar{h}_1$ = effective height of antenna No. 1

$\bar{E}_1$ = incident E-field evaluated at the terminals of antenna No. 1.

We assume here that the incident E-field is parallel to the axis of antenna No. 1. Since the mutual impedance for two perpendicular dipoles is zero, h_1 is the same as the effective height of an isolated dipole. For a half-wave dipole, the value of h_1 measured in the broadside direction is given by

$$\bar{h}_1 = \frac{\lambda}{\pi}\,\hat{z} \quad . \tag{3.2}$$

Since the incidence wave is perpendicular to antenna No. 2, $I_2^{(s)} = 0$.

Denoting the terminal currents and voltages by I_1, I_2 and V_1, V_2, one finds, by the application of the superposition theorem, that

$$I_1 = Y_{11}\bar{h}_1 \cdot \bar{E}_1 + Y_{11} V_1 \tag{3.3}$$

$$I_2 = Y_{22} V_2 \tag{3.4}$$

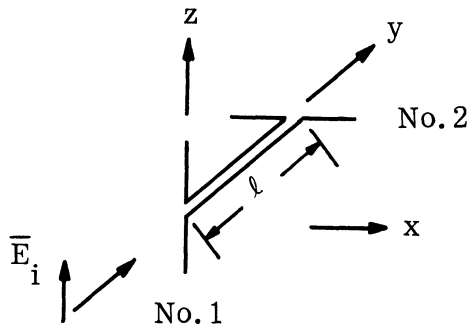

FIG 3-1: PERPENDICULAR DIPOLES LINKED BY A PAIR OF TRANSMISSION LINES

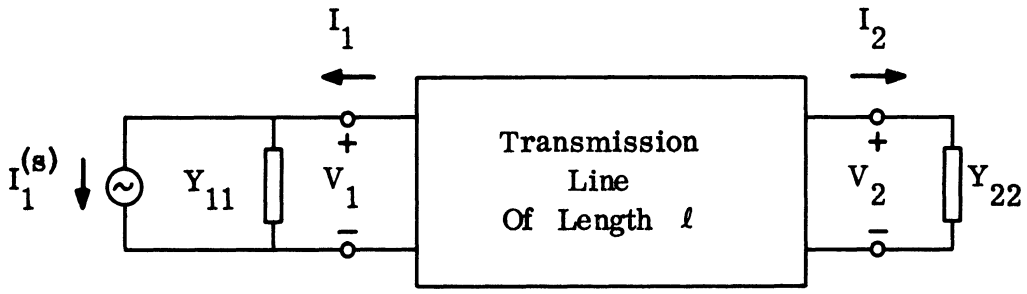

FIG. 3-2: EQUIVALENT CIRCUIT OF DIPOLE PAIR

Because of the constraint due to the transmission line, the terminal currents and voltages must satisfy the following equations:

$$\begin{pmatrix} V_1 \\ V_2 \end{pmatrix} = \begin{pmatrix} Z_a & Z_b \\ Z_b & Z_a \end{pmatrix} \begin{pmatrix} I_1 \\ I_2 \end{pmatrix} \tag{3.5}$$

where

$Z_a = j Z_0 \cot k\ell$

$Z_b = j Z_0 \csc k\ell$

Z_0 = characteristics impedance of the line

ℓ = length of the line

$k = 2\pi/\lambda$ = wave number .

By eliminating V_1 and V_2 in (3.3) and (3.5) we can determine I_1 and I_2. The results are

$$I_1 = Y_{11} \bar{h}_1 \cdot \bar{E}_1 \left[1 - Y_{11} Z_a - Y_{11} Z_b \frac{Y_{22} Z_b}{1 - Y_{11} Z_a} \right]^{-1} \tag{3.6}$$

$$I_2 = \left(\frac{Y_{22} Z_b}{1 - Y_{22} Z_a} \right) I_1 \quad . \tag{3.7}$$

In the case considered in this report, the dipoles are of equal length, so that

$$Y_{11} = Y_{22} = Y = 1/Z \quad . \tag{3.8}$$

In this case we have

$$I_1 = \frac{\bar{h}_1 \cdot \bar{E}_1 (Z - Z_a)}{(Z - Z_a)^2 - Z_b^2} \tag{3.9}$$

and

$$I_2 = \frac{Z_b \bar{h}_1 \cdot \bar{E}_1}{(Z - Z_a)^2 - Z_b^2} \quad . \tag{3.10}$$

It is of interest to calculate the power transferred to the second dipole; it is found by

$$W_2 = |I_2|^2 R \tag{3.11}$$

where $R = \text{Re}\{Z\}$ and is the input resistance of one element. This results in the expression

$$W_2 = \left| \frac{Z_b \bar{h}_1 \cdot \bar{E}_1}{(Z - Z_a)^2 - Z_b^2} \right|^2 R \quad . \tag{3.12}$$

It can be shown that the effective height is related to the directivity and the radiation resistance by the following formula:

$$h^2 = \frac{4\pi D R}{\eta_o k^2} \tag{3.13}$$

where D is the directivity in the broadside direction, and η_o is the free-space characteristic impedance and has the value

$$\eta_o = 120\pi \approx 377 \text{ ohms} \quad .$$

Thus the power transferred to the second antenna is given by

$$W_2 = \frac{4\pi D}{\eta_o k^2} \left| \frac{Z_b R E_1}{(Z - Z_a)^2 - Z_b^2} \right|^2 \tag{3.14}$$

3.2 Optimum Conditions

If the antennas are perfectly matched to the transmission line, i.e. $Z = Z_o$, then

$$I_1 = \frac{h_1 E_1}{2 Z_o} , \tag{3.15}$$

$$I_2 = -e^{-jk\ell} I_1 ,$$

and

$$W_2 = \frac{\pi D \left| E_1 \right|^2}{\eta_o k^2} \tag{3.16}$$

where in general both k and D are frequency - dependent.

There is another case in which high values of transferred power may be expected. Consider a short dipole: its impedance is highly capacitive, and thus $R << \left| X \right|$, and

$$(Z - Z_a)^2 - Z_b^2 \approx -(X - Z_o \cot k\ell)^2 + Z_o^2 \csc^2 k\ell - 2jR(X - Z_o \cot k\ell) . \tag{3.17}$$

The real part vanishes if

$$X = Z_o \frac{(\pm 1 + \cos k\ell)}{\sin k\ell} \tag{3.18}$$

that is, if

$$\frac{X}{Z_o} = \left\{ \begin{array}{l} \cot\left(\frac{k\ell}{2}\right) \\ -\tan\left(\frac{k\ell}{2}\right) \end{array} \right\} \quad . \tag{3.19}$$

The reactance of a short dipole is negative and increases with frequency and thus with increasing k, while the functions of Eq. (3.19) are decreasing. It can be seen that as $k\ell$ increases, the reactance curve will intersect the curve given by $-\tan\left(\frac{k\ell}{2}\right)$ first and then alternately intersect the two curves. As k or frequency increases, the dipole is no longer short, its input resistance can no longer be ignored, and this approach breaks down. Thus Eq. (3.19) is only valid for the condition

$$k\ell < \frac{2\pi\ell}{c} f_o$$

where f_o is the highest frequency for which

$$R << |X| \quad .$$

In this case, we get

$$W_2 = \frac{\pi D |E_1|^2}{\eta_o k^2} \tag{3.20}$$

and

$$I_2 = \frac{I_1}{\pm 1 - jR/Z_o} \approx \pm I_1 \quad , \tag{3.21}$$

where the negative sign corresponds to the second form of Eq. (3.19).

3.3 An Example

An example will now be worked out which illustrates these relations. Consider a transmission line of length ℓ and characterisitic impedance of 200Ω, terminated at the ends with perpendicularly oriented dipoles of length L. Assume further that the dipoles are cylindrical and have a thickness parameter Ω of 10, corresponding to length-to-radius ratio of $L/r = 75$. Then the reactance as a function of frequency can be found in the results of King (1956). The functions of the right-hand side of Eq. (3.19) are plotted against the variable ℓ/λ in Fig. 3-3, along with the reactances of dipoles corresponding to lengths $L_1 = \frac{3\ell}{4}$, $L_2 = \frac{3\ell}{8}$, $L_3 = \frac{3\ell}{16}$.

The first intersection of the reactance curve for L_1 with the tangent curve occurs at point 1, corresponding to $\ell/\lambda = .234$ and $X_1 = 190\Omega$. The shorter dipoles of lengths L_2 and L_3 have resonances at higher frequencies, and L_3 in particular has two resonances in the region where it is still electrically short. The dashed line at -200Ω indicates the region where the short dipole assumption breaks down.

The intersection points can also be interpreted as resonances corresponding to a fixed length of dipole while the spacing ℓ varies in the ratio 1:2:4. More specifically, let $\ell_1 = 2.5$ cm, so that L = 1.875 cm and the transmission line is a quarter-wavelength long at 3 GHz. Then the first resonance (point 1) occurs at 2.8 GHz, where the reactance is -180Ω. The percent bandwidth can be estimated as 100 percent x $R/|X|$, where R is given approximately by

$$R = 80\pi^2 \left(\frac{L}{\lambda}\right)^2 .$$

The results are tabulated in Table III-1 for points 1-5 of the figure.

It can be seen that as the spacing between the dipoles increases, the resonant frequency decreases, and the percent bandwidth decreases markedly.

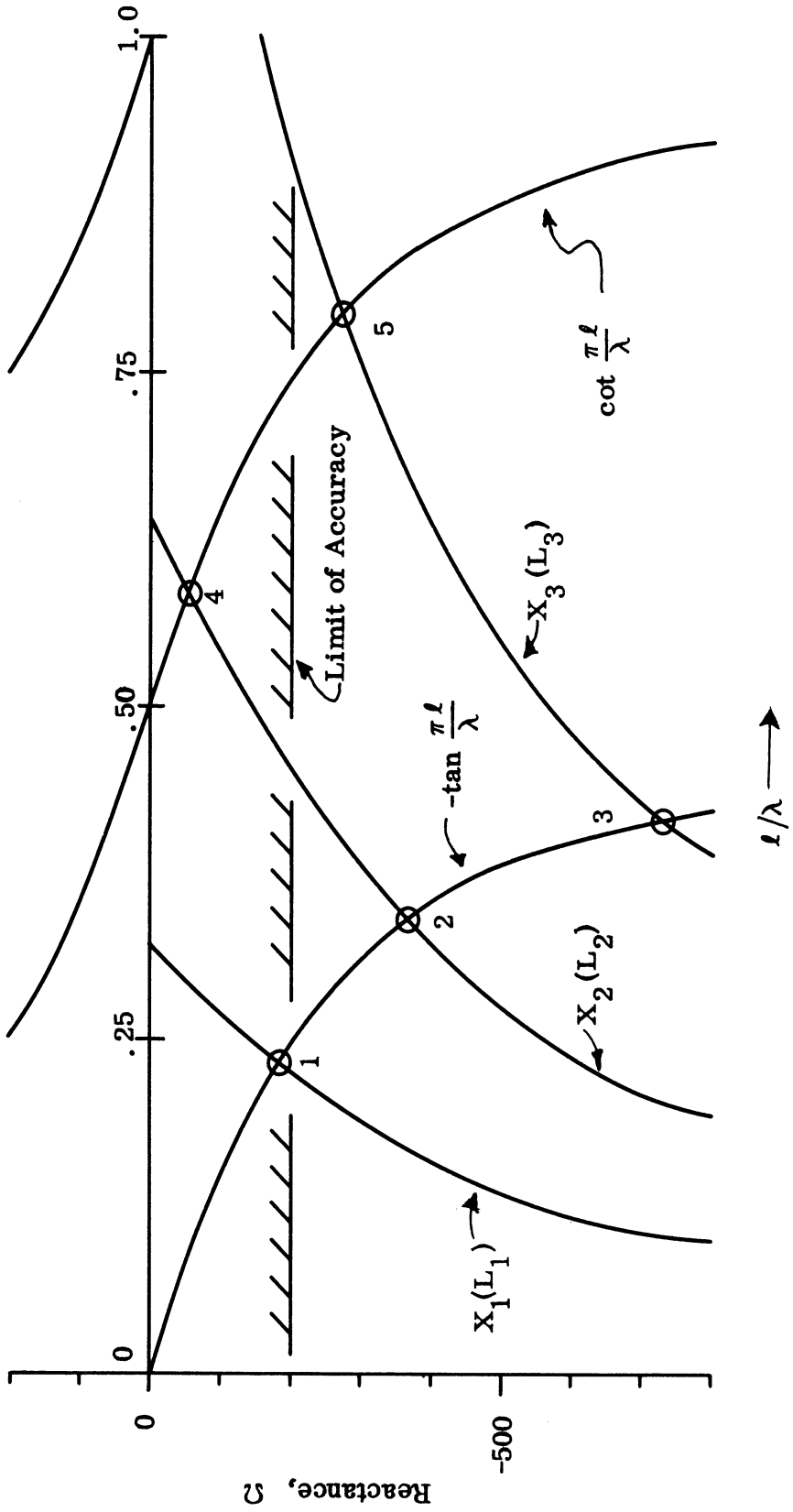

FIG. 3-3 : GRAPH FOR DETERMINATION OF CRITICAL FREQUENCIES IN EXAMPLE PROBLEM.

3.4 Scattered Fields of Dipole Pair

It can be seen from this discussion that the scattered field of each dipole element is of comparable strength at the optimum conditions, since the currents are of comparable magnitude. For equal length dipoles, the scattered field is given by

$$\bar{E}_n^{(s)} = \frac{j\eta_o I_n}{2\pi} \frac{e^{-jkR_n}}{R_n} P(\theta_n)\hat{\theta}_n \tag{3.22}$$

where $P(\theta_n)$ is the antenna pattern factor depending on the angle θ_n; n = 1 or 2, and θ_1 and θ_2 denote, respectively, the angle between the direction of observation and the axis of the dipole. For the configuration of Fig. 3-1 the forward scattered wave, for which $\theta_1 = \theta_2 = 90^o$, $\hat{\theta}_1 = -\hat{z}$, $\hat{\theta}_2 = \hat{x}$, is given by

$$\bar{E}^{(s)} = \bar{E}_1^{(s)} + \bar{E}_2^{(s)}$$

$$= \frac{-j\eta_o I_1}{2\pi} P(\pi/2) \frac{e^{-jkR_1}}{R_1} \left[\hat{z} - \hat{x} e^{jk\ell} \frac{I_2}{I_1}\right] . \tag{3.23}$$

From the bracketed quantity we can deduce the polarization characteristics of the forward scattered wave. For the case $Z = Z_o$, Eq. (3.16) gives the relation between the currents, and we get

$$[\ ] = [\hat{z} + \hat{x}] \tag{3.24}$$

for the bracketed quantity of (3.23). This represents a linearly polarized wave tilted clockwise 45^o from the z-axis. For the conditions of Eq. (3.19), and using Eq. (3.21), we get

Point	Spacing ℓ, cm.	Resonant Freq. GH_z	Reactance, Ω	Resistance, Ω	% Bandwidth
1	2.5	2.8	-180	24.2	13.5
2	5	1.82	-360	10.2	2.8
3	5	1.12	-730	3.88	0.53
4	10	(Not a short dipole)----------			
5	10	2.38	-270	17.5	6.5

TABLE III-1: PROPERTIES OF DIPOLE PAIR, EXAMPLE PROBLEM

$$[\ ] = \left[\hat{z} \pm \hat{x} e^{jk\ell}\right] . \tag{3.25}$$

The lowest resonance frequency corresponds to the lower sign. In this case the forward scattered wave is elliptically polarized with a counterclockwise (left) sense for $k\ell < \pi$, with the major axis tilted clockwise from the z-axis. For the condition $k\ell = \pi/2$ left circular polarization is achieved. For the second resonance, the scattered wave is clockwise (right) with a counterclockwise tilt. A similar analysis for the backscattered wave indicates, for the first resonance, a counterclockwise sense of polarization rotation, just as for the forward scattered wave.

From this discussion it is evident that the scattered wave can be circularly polarized if the transmission line length is an odd multiple of a quarter wavelength. In its application to the radant configuration, however, the incident field also enters into the total field, and cannot be ignored. In general, the total field is difficult to predict.

IV

PROPERTIES OF A SINGLE DIPOLE ON A DIELECTRIC SHEET

The radant panel has two sheets, each having a thickness of 1/16 inches, on which the dipoles are etched. The transmission efficiency of each sheet for an incident plane wave is approximately 98 percent for angles of incidence up to 75^{o} away from normal. However, while the effect of the sheets as radome panels is very small, the impedance of the dipoles is changed markedly by their presence. It was decided that an experimental measurement of a single dipole element would be more expedient than an analytic investigation.

4.1 Dipole Impedance

Figure 4-1 shows the results of the impedance measurement of a printed circuit dipole of width 1/16 inches and overall length of 1.3 inches, etched on a fiberglass board of dimensions 4 inches x 4 inches x 1/16 inches, The center of the chart (1. + j0.) corresponds to 160Ω, which is the characteristic impedance of the two-wire transmission line joining the two dipole arrays. Without the dielectric the dipole would be resonant at about 4.3 GHz with a resistance of 73Ω; with the dielectric it is resonant at about 3.0 GHz with a resistance of 48Ω. A second resonance takes place at 3.8 GHz with a resistance of 160Ω, which is the maximum value of resistance. The latter point corresponds exactly to the perfectly matched condition of Eqs. (3.15) and (3.16).

The balun used was an adjustable half-wave-line type, reset for each frequency used. (See Fig. 4-2).

4.2 Critical Frequencies

At 3.8 GHz where there is a perfect match one would expect an optimum transfer of power to the second dipole. This is subject to errors arising from the finite extent of the dielectric sheet and to the mutual impedance effects of neighboring

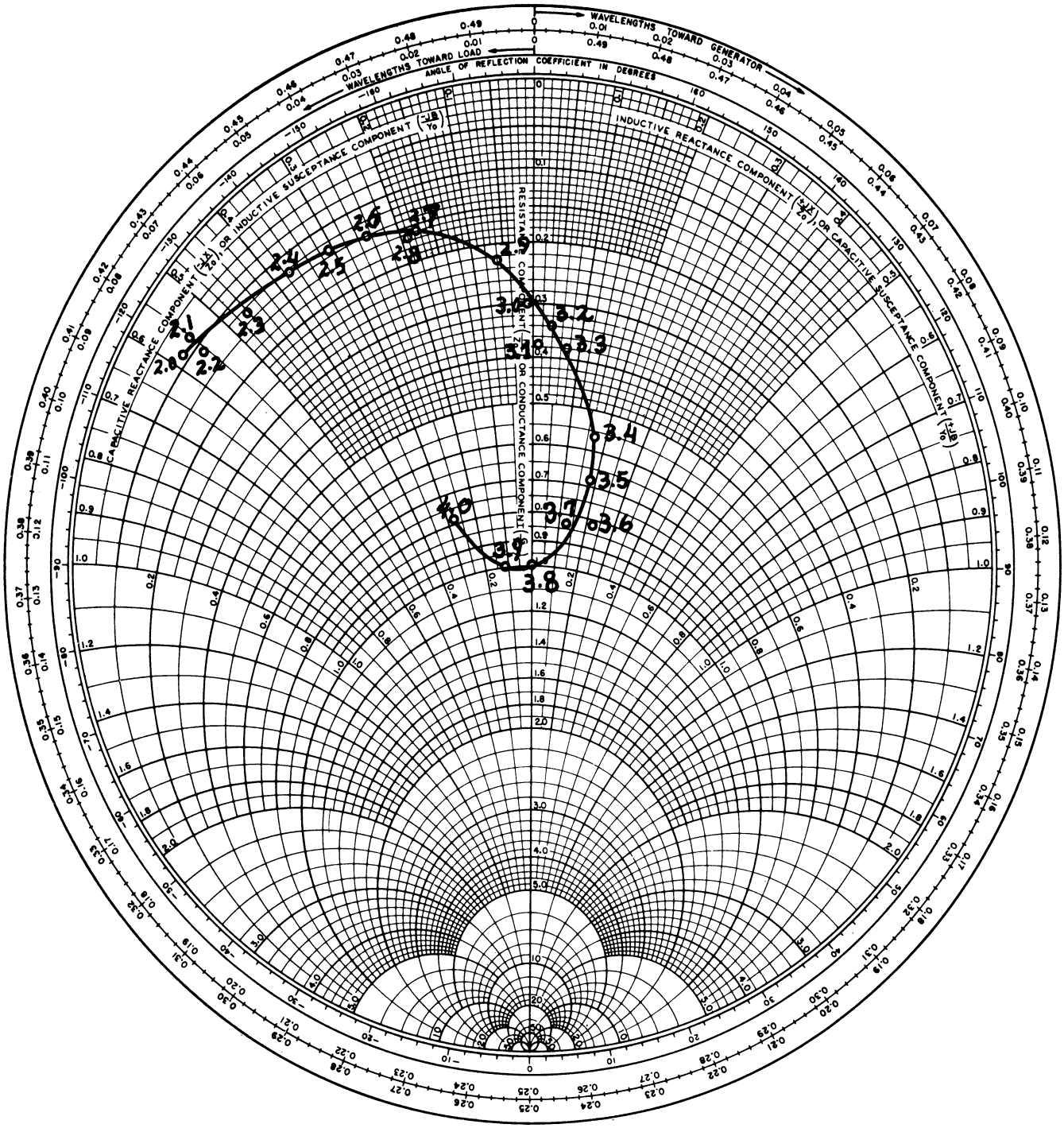

FIG. 4-1: DIPOLE IMPEDANCE

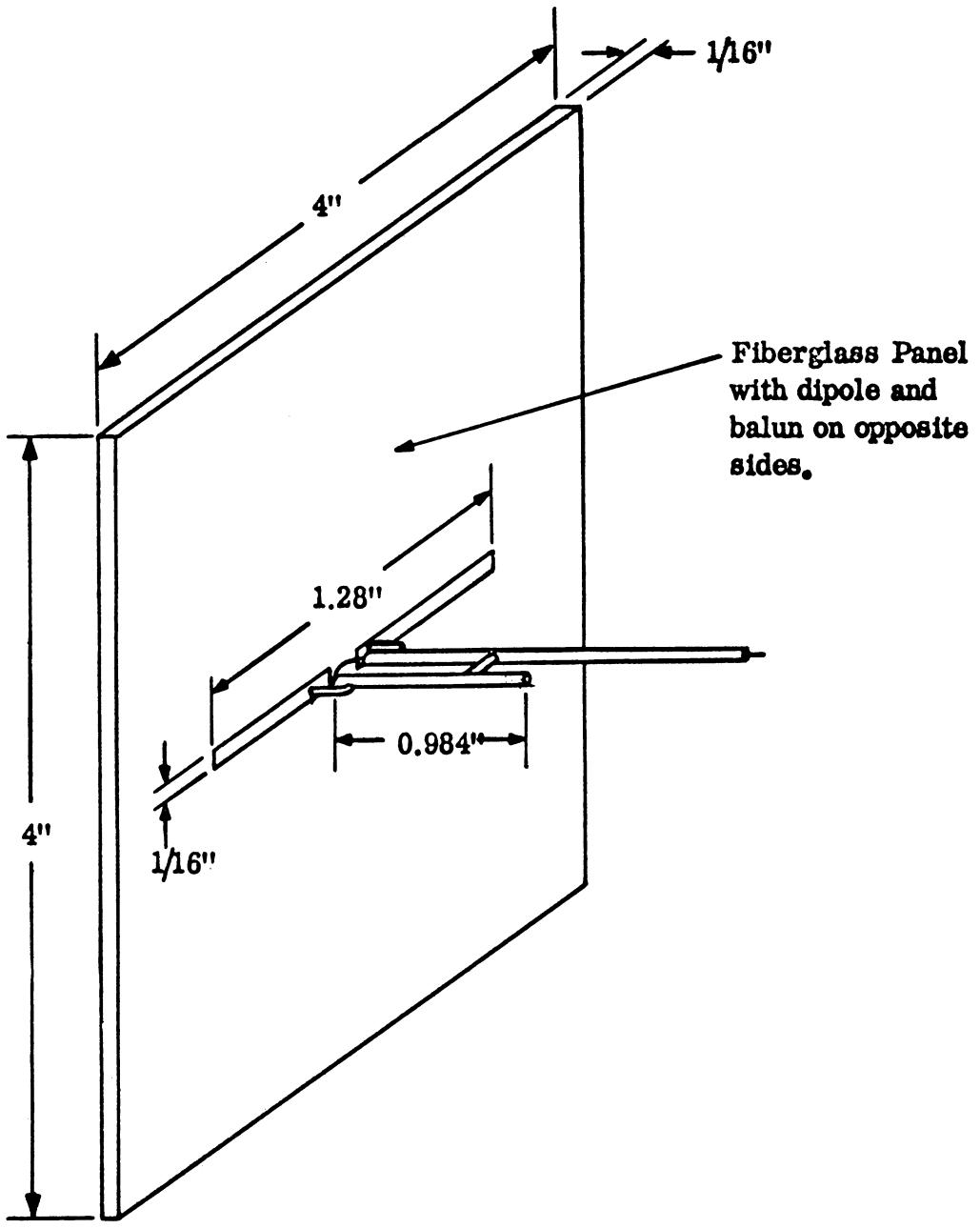

FIG. 4-2: DIPOLE ELEMENT AND BALUN

dipole elements of the array. The discussion of resonant frequencies for short dipoles in Eq. (3.19) will not be applicable to this particular geometry for frequencies above 2.6 GHz but should indicate any resonances below that frequency. In Fig. 4-3 the resistance and reactance are plotted for frequencies up to 3 GHz, including some points extrapolated down to 1.5 GHz. Also plotted is the function $(-\tan\frac{k\ell}{2})$ where ℓ = 1 inch. The intersection of the reactance curve with this function occurs at approximately 2.0 GHz. Thus there are at least two frequencies below 4 GHz where the scattered field should be large.

4.3 Power Transferred as a Function of Frequency

In order to get a better idea of the behavior of the scattered field of the second dipole element as a function of frequency it is necessary to know more about the effective height of the elements. From Eq. (3.13) it is evident that if the directivity of the elements is known, the effective height can be calculated, and the power transferred to the second antenna follows from Eqs. (3.12) or (3.14). In the next paragraph, it will be shown that the directivity does not change appreciably for frequencies less than 4.0 GHz. This allows a straightforward estimate of transferred power to be obtained.

Consider a dipole of half-length L having a current distribution

$$I(z') = I_o \sin\left[k_1 (L - z')\right] \tag{4.1}$$

where k_1 is not in general equal to $2\pi/\lambda$. The far field is given by

$$\bar{E}(\bar{R}) = \frac{j\eta_o I_o}{2\pi} \frac{e^{-jkR}}{R} P(\theta)\hat{\theta} \tag{4.2}$$

where

$$P(\theta) = \frac{\sin\theta}{1 - \alpha^2 \cos^2\theta} \left[\cos(\alpha k_1 L \cos\theta) - \cos(k_1 L)\right] \tag{4.3}$$

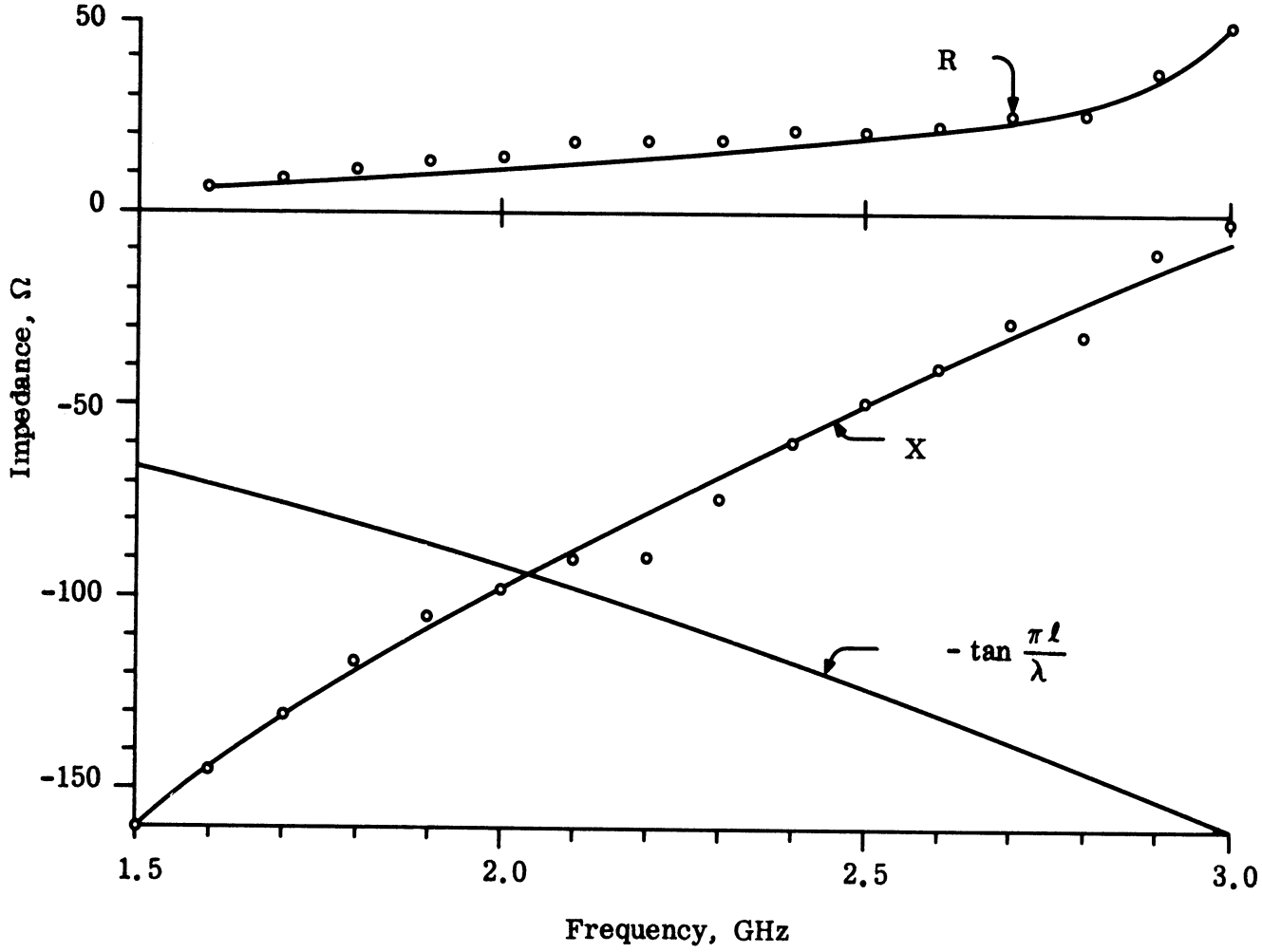

FIG. 4-3 : DIPOLE IMPEDANCE AND DETERMINATION OF CRITICAL FREQUENCY.

and $k = \alpha k_1 = 2\pi/\lambda$ is the free-space wave number, and k_1 is determined by the impedance of the antenna and accounts for the effect of the dielectric. The simplifying assumption is made here that the antenna is still omnidirectional. For our case we expect the current distribution of a full-wave dipole at 3.8 GHz, and thus $k_1 L = \pi$ at this frequency, or

$$\alpha = \frac{k}{k_1} = .417 \ .$$

$P(\theta)$ is maximum at $\theta = 90^o$ and has a half-power beamwidth of 77^o. This is approximately the same as a half-wave antenna in free space, which has a beamwidth of 78^o. Thus the directivity will not differ greatly from that of a half-wave dipole, namely

$$D_{max} = 1.64 \ .$$

For a half-wave current distribution at 3 GHz, $\alpha = .658$, and the beamwidth is 84^o, compared with the short dipole beamwidth of 90^o. This is plotted in Fig. 4-4 along with the estimated directivity. Thus the assumption of a constant directivity of 1.5 over the frequency range 0-4 GHz will not incur an error of more than 0.3 db in transferred power.

The effective height can be found from Eq. (3.13) for $D = 1.5$ to be

$$h = \frac{1}{k}\sqrt{\frac{R}{20}} \ . \qquad (4.4)$$

This is plotted in Fig. 4-5 as a function of frequency. The straight line represents the actual value of L, which is 1.65 cm. The dashed line is the effective height of the same dipole in free space.

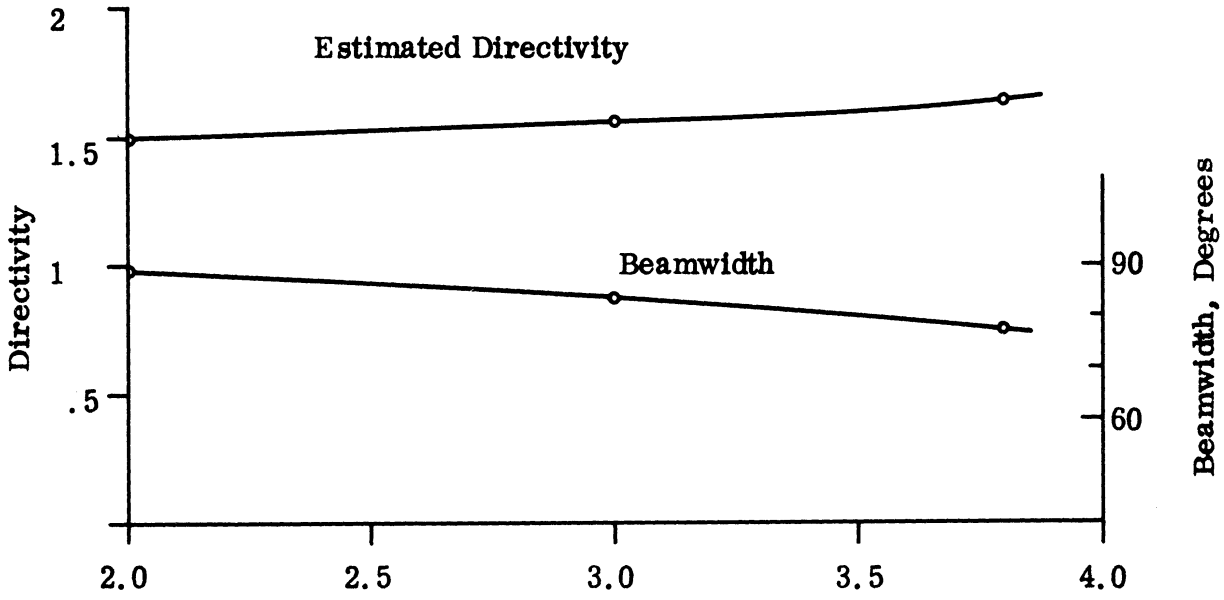

FIG. 4-4 : CALCULATED DIRECTIVITY AND BEAMWIDTH OF DIPOLE ELEMENT

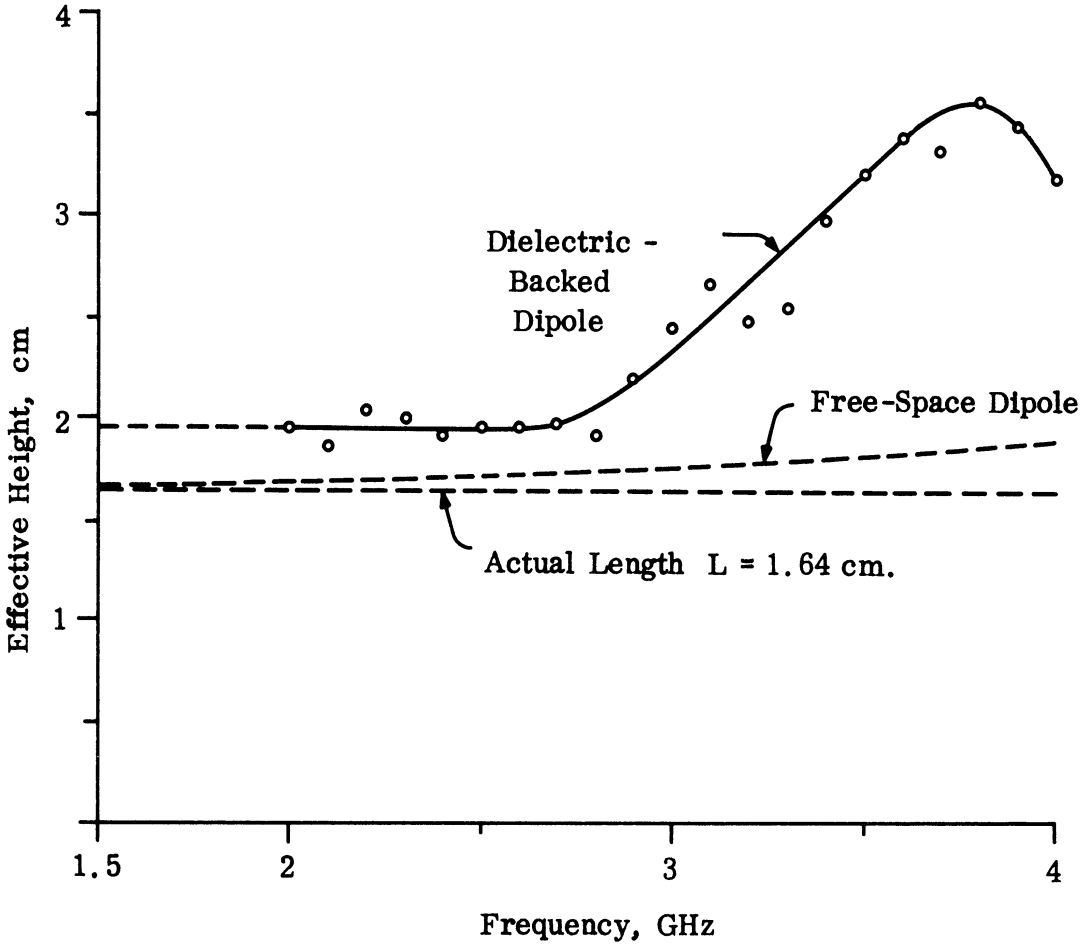

FIG. 4-5 : EFFECTIVE HEIGHT OF DIPOLE ELEMENT

For convenience, let us define W_o as the total power reradiated by both dipoles when $Z = Z_o$ at 3.8 GHz. Then

$$W_o = \frac{2\pi D |E_1|^2}{\eta_o k_o^2} ,$$

where k_o is the free-space wave number at 3.8 GHz. From Eq. (3.14) we can write, for D assumed constant,

$$N = \frac{W_2}{W_o} = 2\left(\frac{k_o}{k}\right)^2 \left| \frac{Z_b R}{(Z - Z_a)^2 - Z_b^2} \right|^2$$

or

$$N = 2\left(\frac{3.8}{f}\right)^2 \left| \frac{Z_b^2}{(Z - Z_a)^2 - Z_b^2} \right|^2 \qquad (4.6)$$

where f is the frequency in GHz. Thus N gives a measure of the relative power transferred to the second element and reradiated over the frequency band for a given incident power density level. Note that N may exceed unity. The function N is plotted against frequency in Fig. 4-6. The resonance near 2 GHz is evident along with the maximum at 3.6 GHz, although the latter is not sharp. On the basis of the single dipole element model and the theory, one would expect a narrow-band resonance at 2 GHz and a broader band resonance at 3.6 GHz when these elements are used in the radant array. Since the directivity of the panel increases with frequency, it would be anticipated that the horizontally polarized signal radiated by the second dipole panel would be comparable at the two frequencies.

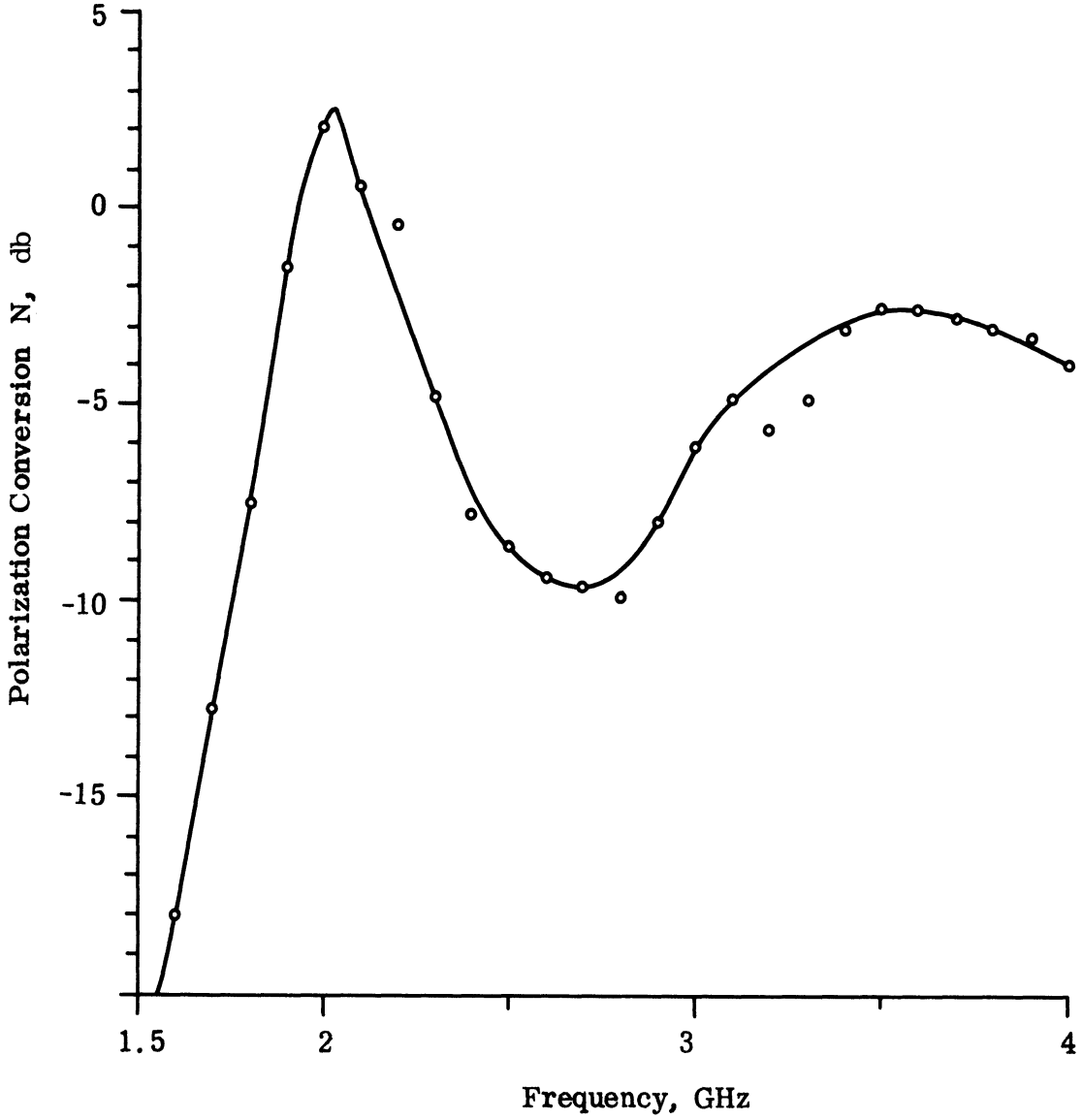

FIG. 4-6 : POLARIZATION CONVERSION FACTOR N

V

EXPERIMENTAL RESULTS OF RADANT PANEL

The experimental program for testing the radant panel involved measuring patterns of the receiving horn-radant panel assembly for an initial spacing of 15 inches at 100 MHz increments up to 4 GHz. At promising frequency ranges, additional data was taken, varying the spacing and investigating the polarization characteristics. The properties to be studied included pattern beamwidth, bandwidth, axial ratio of ellipticity, side-lobe level, and "transmission coefficient". The "transmission coefficient" is defined as the ratio of the signal obtained, with a given receiver polarization and the radant panel present, to the signal obtained with matched polarization and no radant panel present. This is always taken at normal incidence.

5.1 Patterns of the Horn-Radant Assembly

Patterns were taken with a vertically polarized transmitting horn of the receiving horn-radant panel assembly in the ϕ-plane of Fig. 2-5. Thus the patterns correspond to H-plane cuts for incident and like-polarized signals, and to E-plane cuts for the cross-polarized configuration. The power level was monitored by means of a directional coupler, as shown in the block diagram of Fig. 5-1. The distance between transmitting horns is 70 ft., which satisfies the far field criterion of the horns and radant for the frequencies of interest. The patterns are shown in Figs. 5-2 and 5-3 for the cross-polarized configuration. In Fig. 5-3 the panel is reversed from Fig. 5-2. Table V-1 indicates the notation used. The relative scales of the patterns are similar, within about 2 db over the frequency band 2.2-4.2 GHz. The level of signal below 2.1 GHz for the cross-polarized case was below the limit of the range. In this frequency range L-band horns were used.

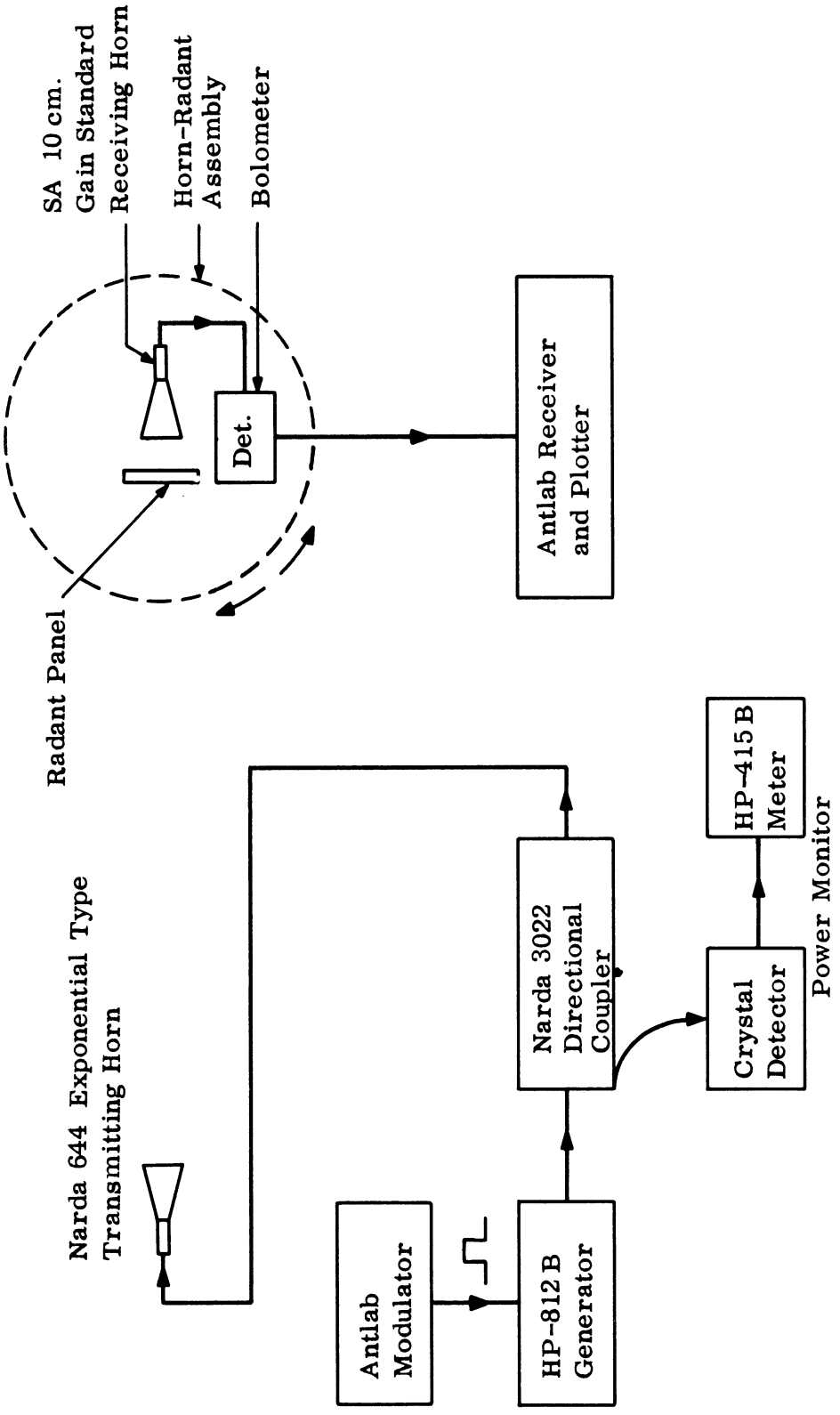

FIG. 5-1: BLOCK DIAGRAM OF MEASUREMENTS

TABLE V-1: CONFIGURATION DESIGNATION

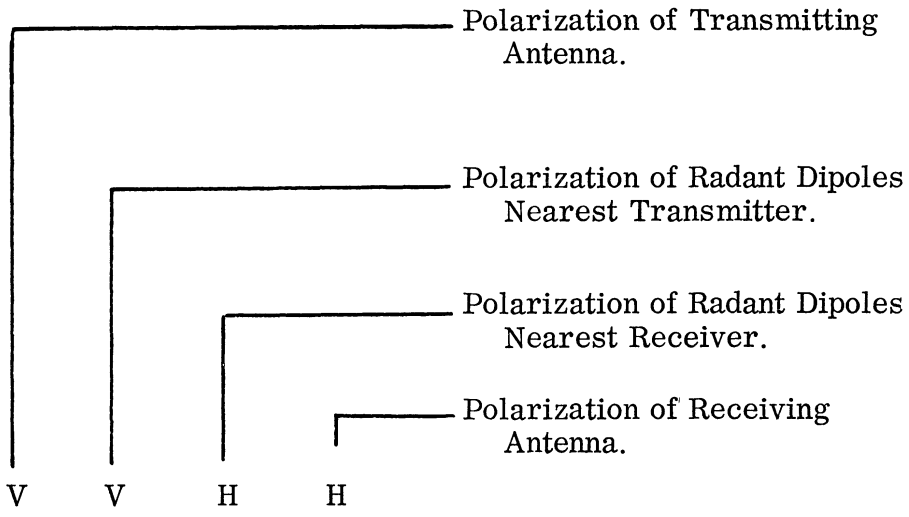

X- Indicates a Parameter or Variable

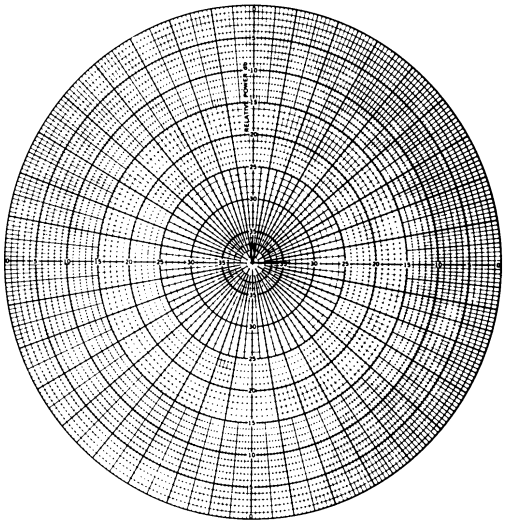

(a) f = 2.1 GHz

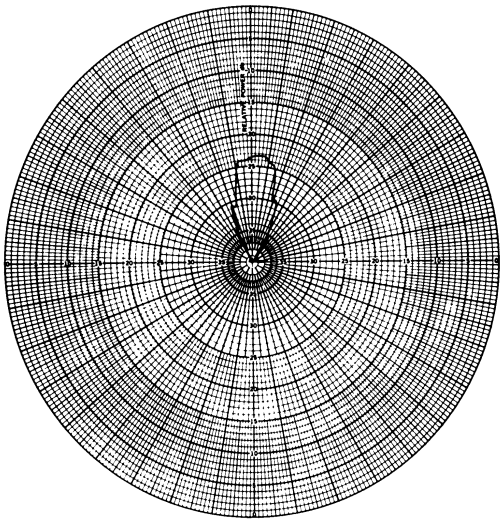

(b) f = 2.2 GHz

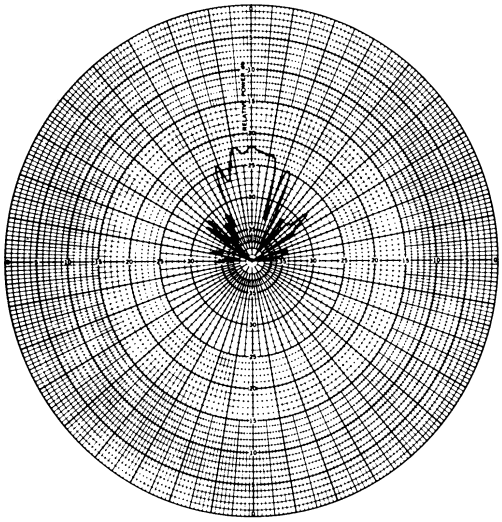

(c) f = 2.3 GHz

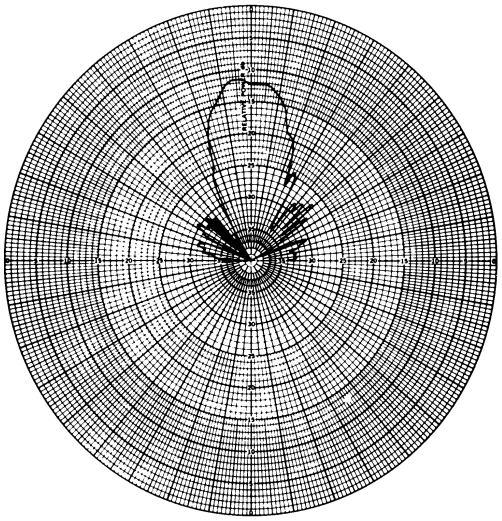

(d) f = 2.4 GHz

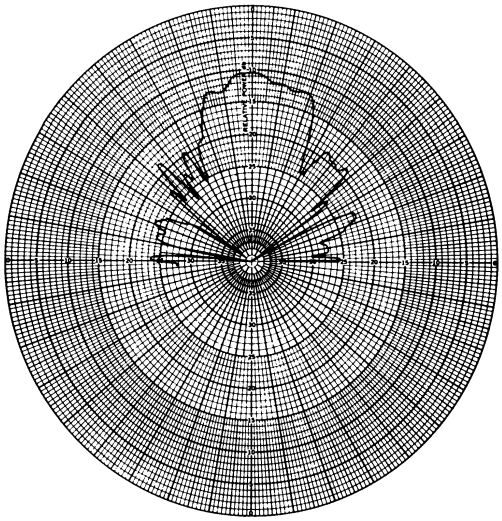

(e) f = 2.5 GHz

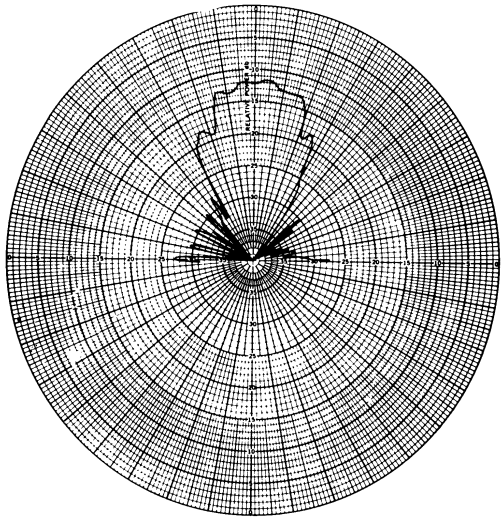

(f) f = 2.6 GHz

FIG. 5-2a-f: CROSS-POLARIZED PATTERNS OF HORN-RADANT ASSEMBLY, VVHH, 15 in. SPACING.

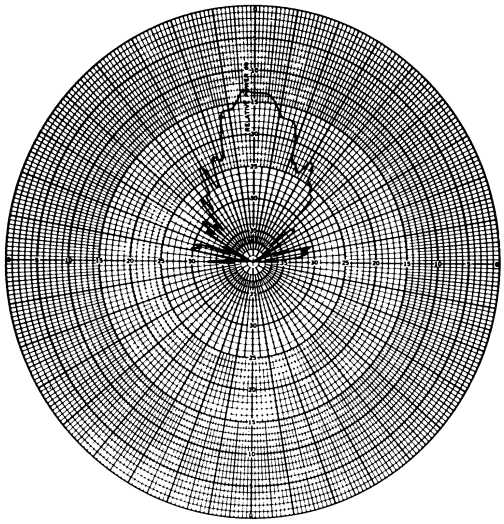

(g) f = 2.7 GHz

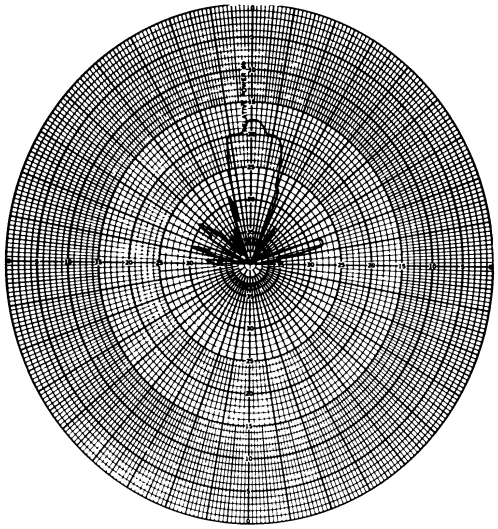

(h) f = 2.8 GHz

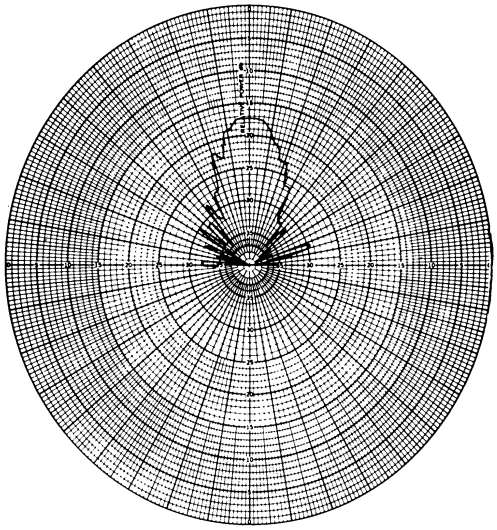

(i) f = 2.9 GHz

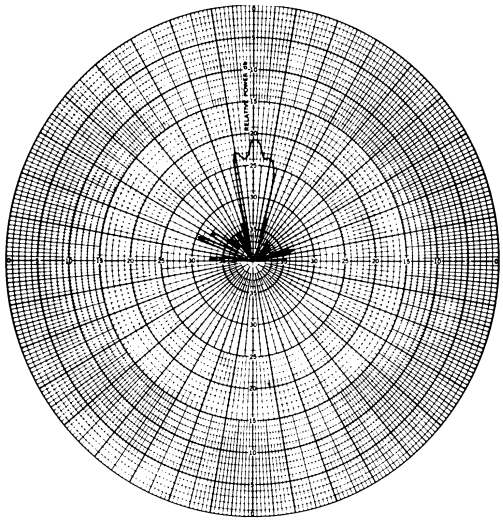

(j) f = 3.0 GHz

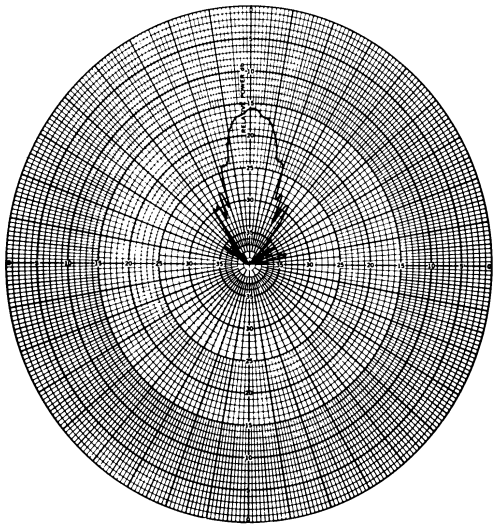

(k) f = 3.1 GHz

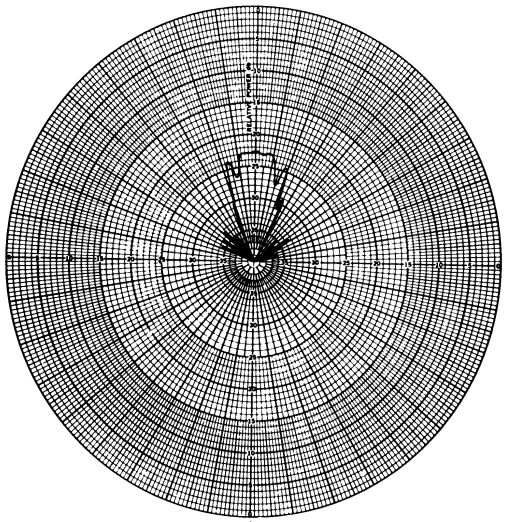

(l) f = 3.2 GHz

FIG. 5-2g-1: CROSS-POLARIZED PATTERNS OF HORN-RADANT ASSEMBLY, VVHH, 15 in. SPACING.

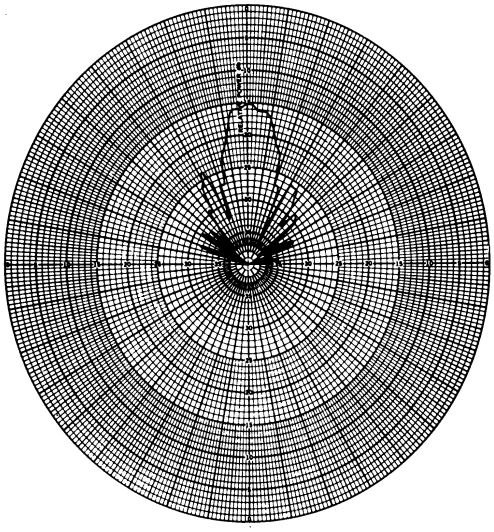

(m) f = 3.3 GHz

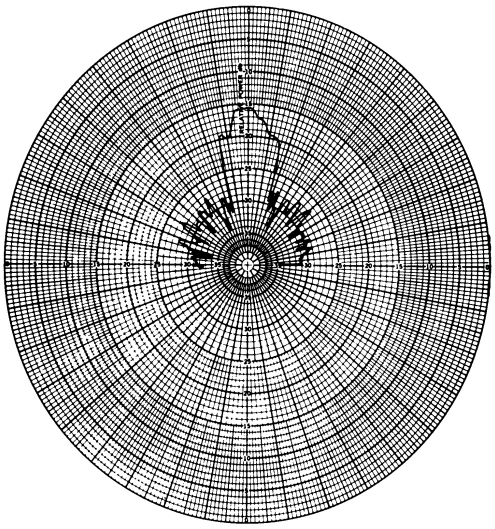

(n) f = 3.4 GHz

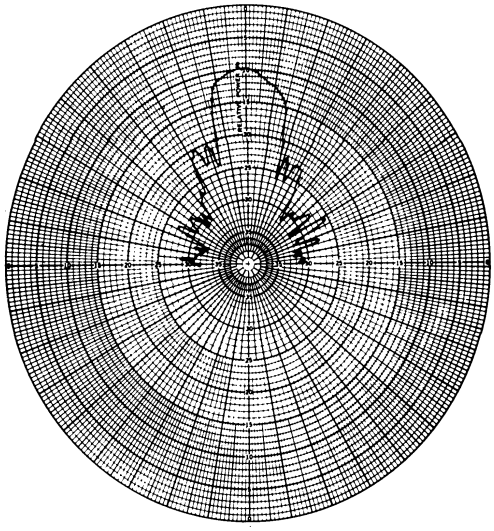

(o) f = 3.5 GHz

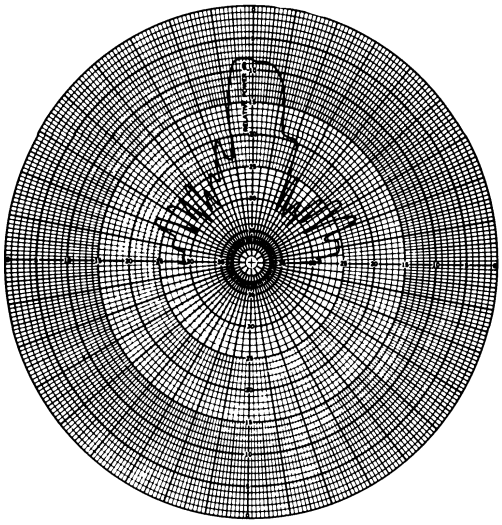

(p) f = 3.6 GHz

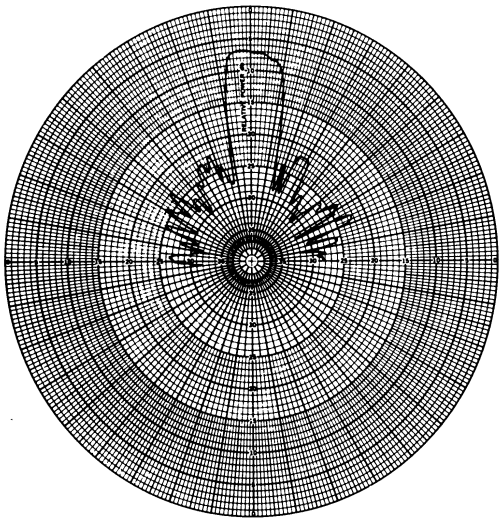

(q) f = 3.7 GHz

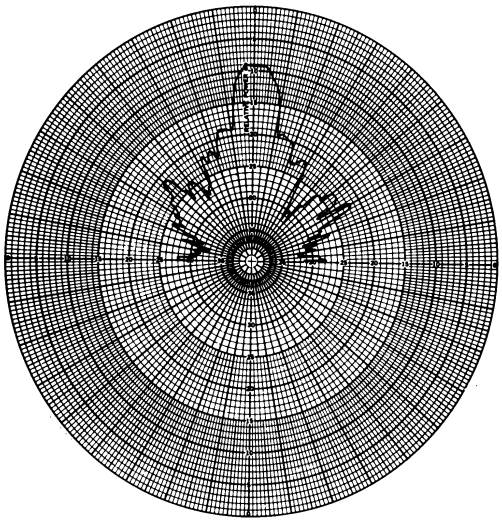

(r) f = 3.8 GHz

FIG. 5-2m-r: CROSS-POLARIZED PATTERNS OF HORN-RADANT ASSEMBLY, VVHH, 15 in. SPACING.

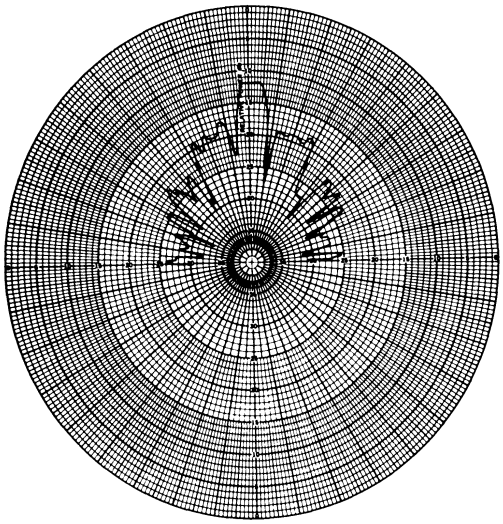

(s) f = 3.9 GHz

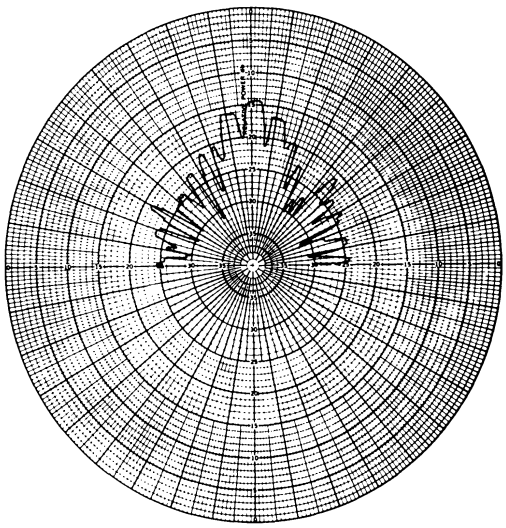

(t) f = 4.0 GHz

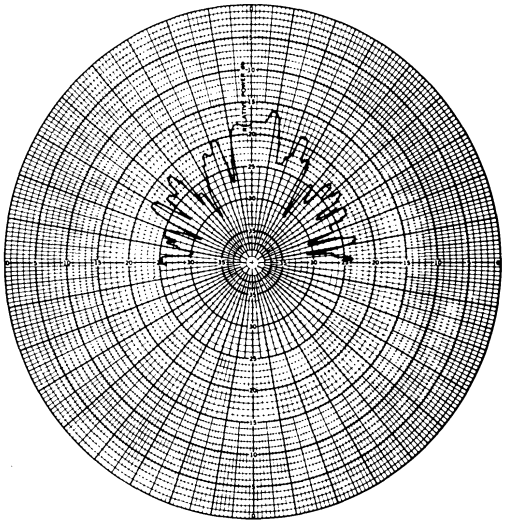

(u) f = 4.1 GHz

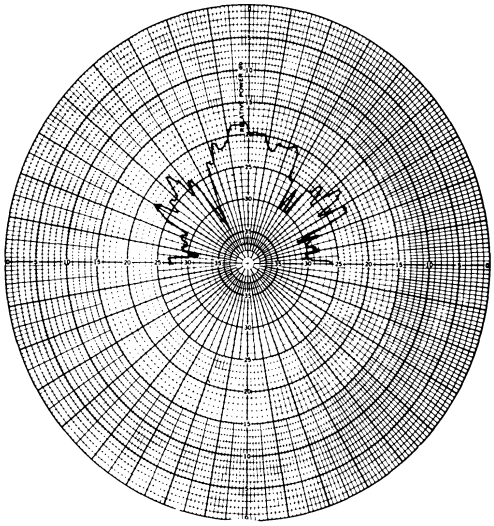

(v) f = 4.2 GHz

FIG. 5-2s - v: CROSS-POLARIZED PATTERNS OF HORN-RADANT ASSEMBLY, VVHH, 15 in. SPACING.

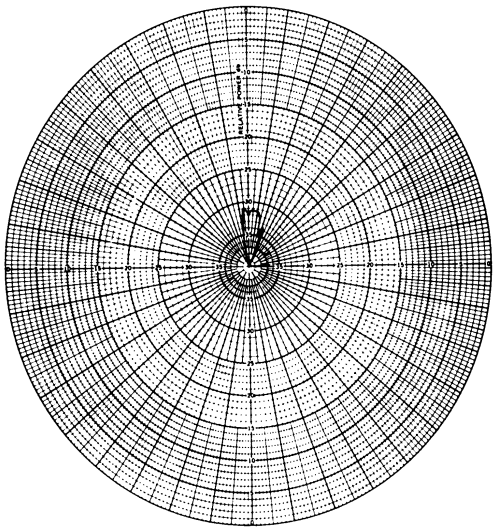

(a) f = 2.1 GHz

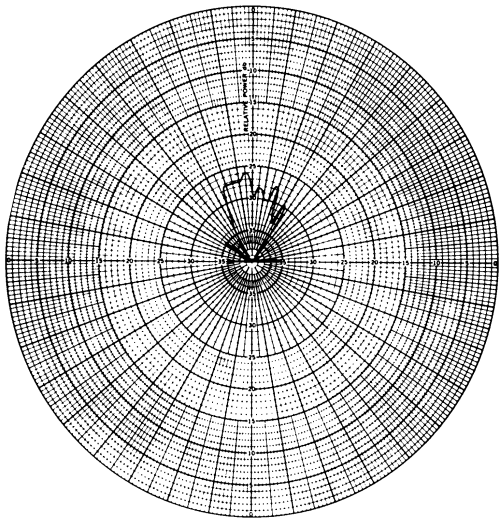

(b) f = 2.2 GHz

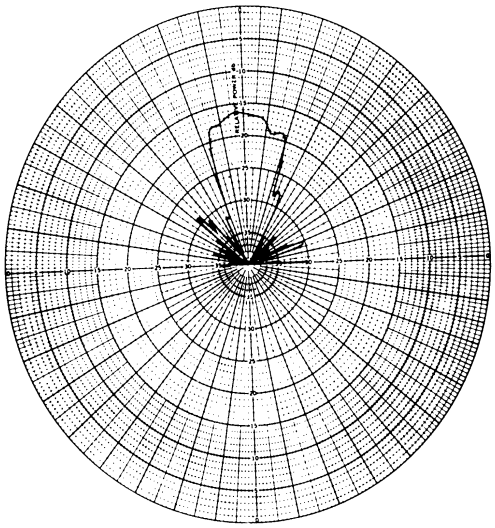

(c) f = 2.3 GHz

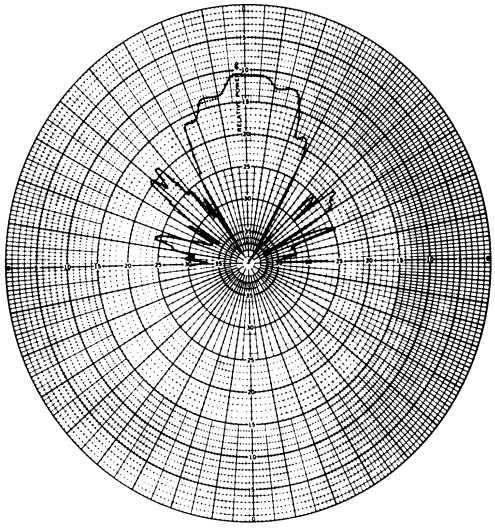

(d) f = 2.4 GHz

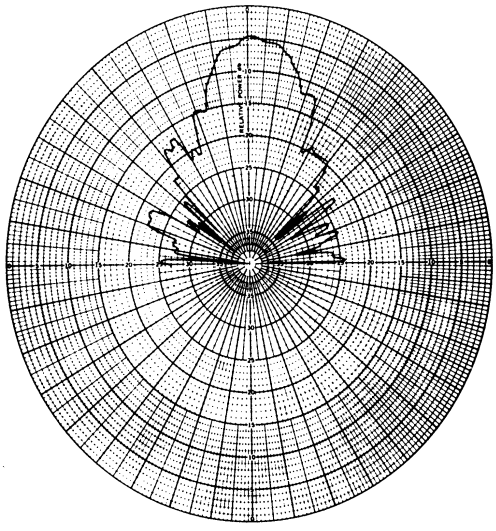

(e) f = 2.5 GHz

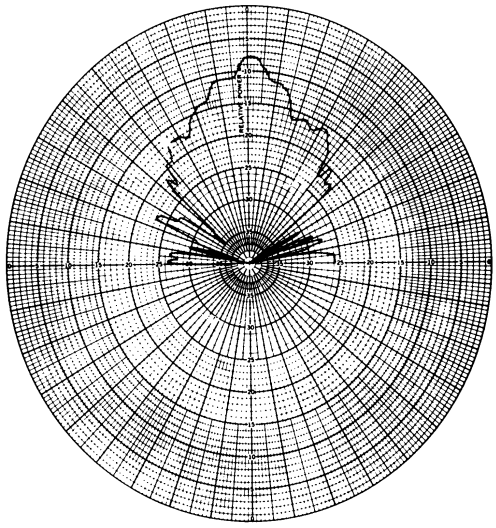

(f) f = 2.6 GHz

FIG. 5-3a-f: CROSS-POLARIZED PATTERNS OF HORN-RADANT ASSEMBLY, VHVH, 15 in. SPACING.

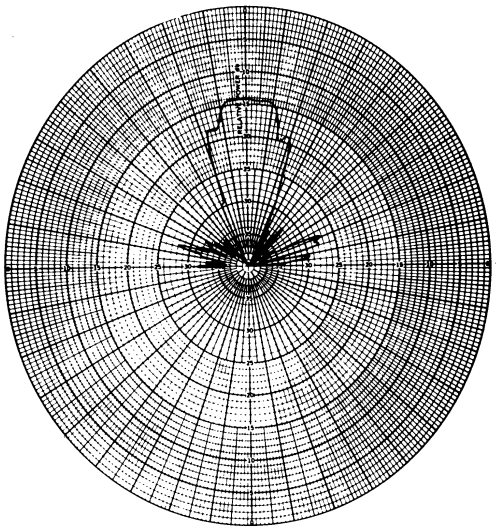

(g) f = 2.7 GHz

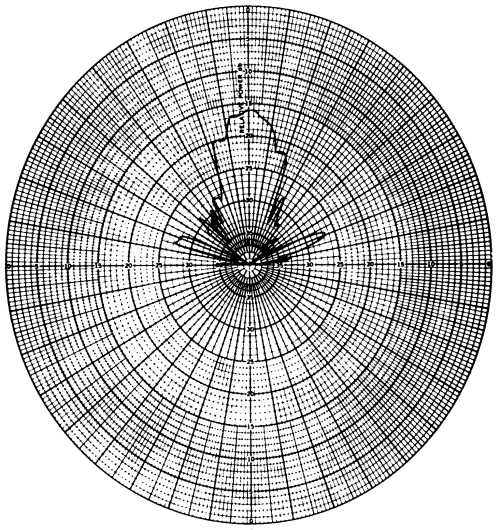

(h) f = 2.8 GHz

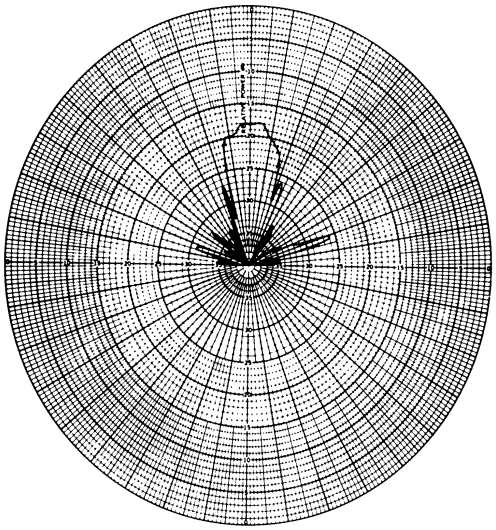

(i) f = 2.9 GHz

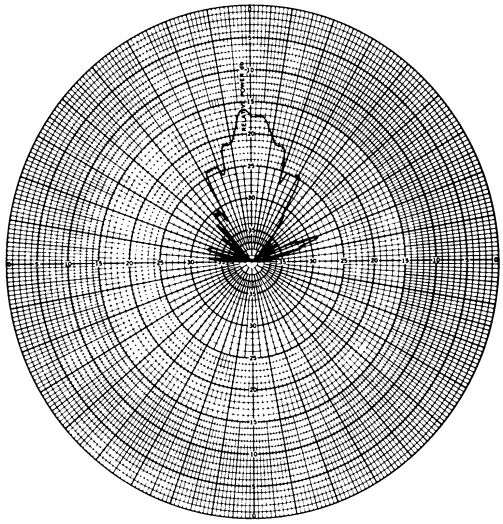

(j) f = 3.0 GHz

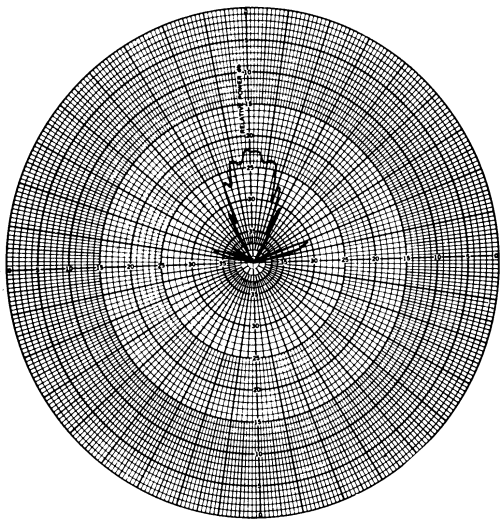

(k) f = 3.1 GHz

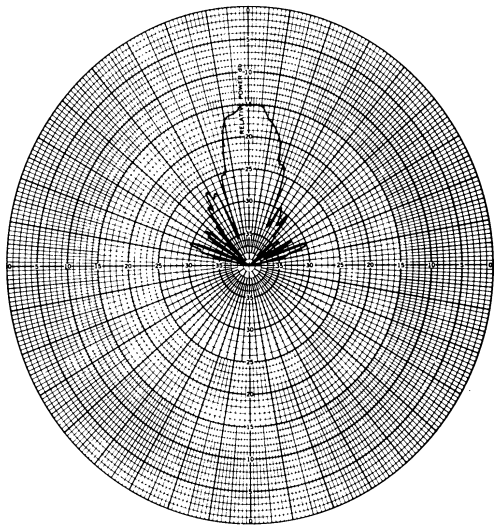

(l) f = 3.2 GHz

FIG. 5-3g - l: CROSS-POLARIZED PATTERNS OF HORN-RADANT ASSEMBLY, VHVH, 15 in. SPACING

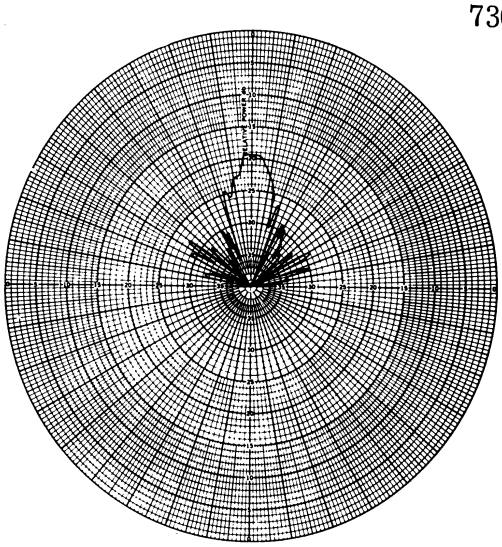

(m) f = 3.3 GHz

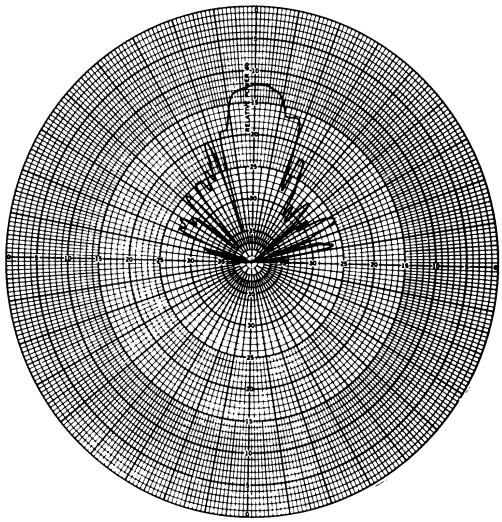

(n) f = 3.4 GHz

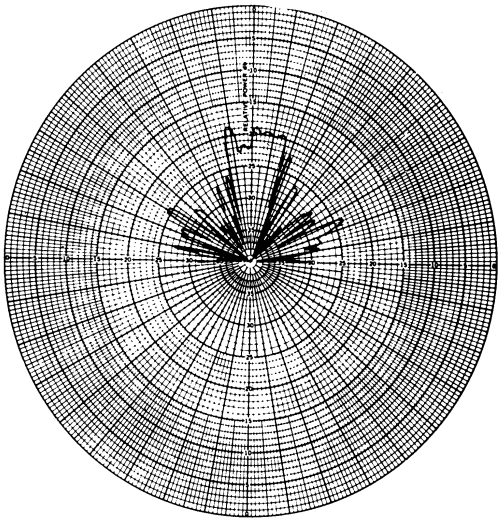

(o) f = 3.5 GHz

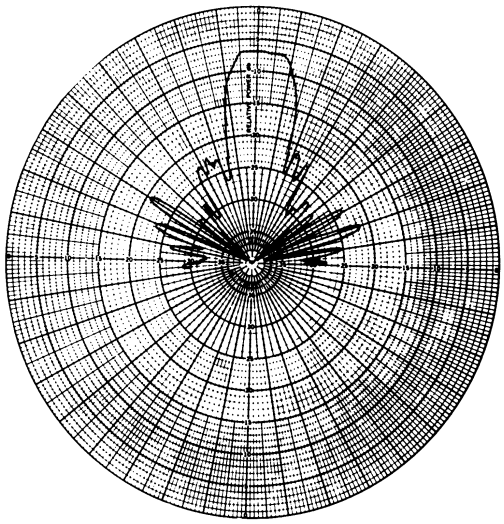

(p) f = 3.6 GHz

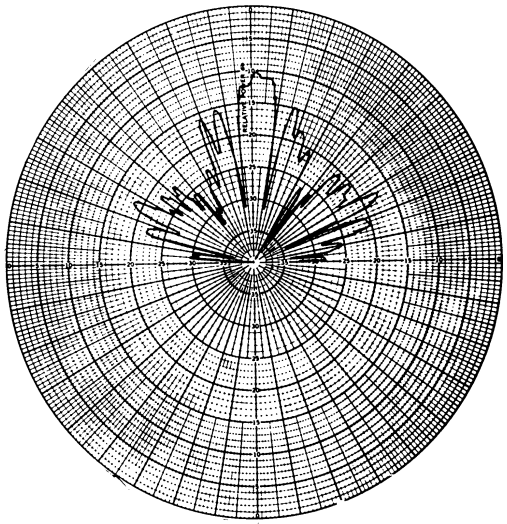

(q) f = 3.7 GHz

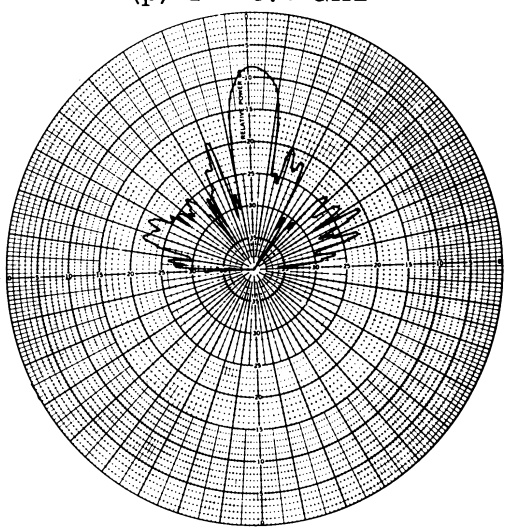

(r) f = 3.8 GHz

FIG. 5-3m-r: CROSS-POLARIZED PATTERNS OF HORN-RADANT ASSEMBLY, VHVH, 15 in. SPACING.

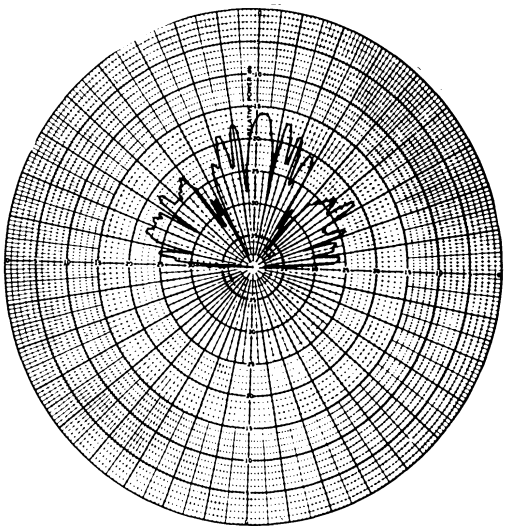

(s) f = 3.9 GHz

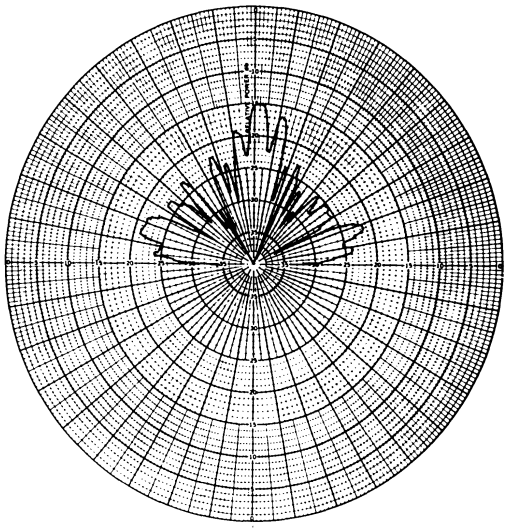

(t) f = 4.0 GHz

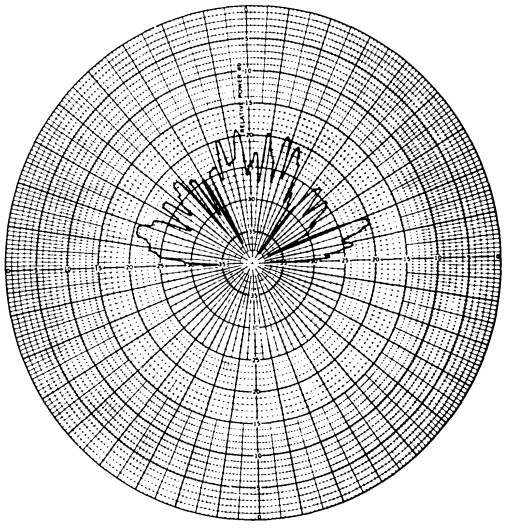

(u) f = 4.1 GHz

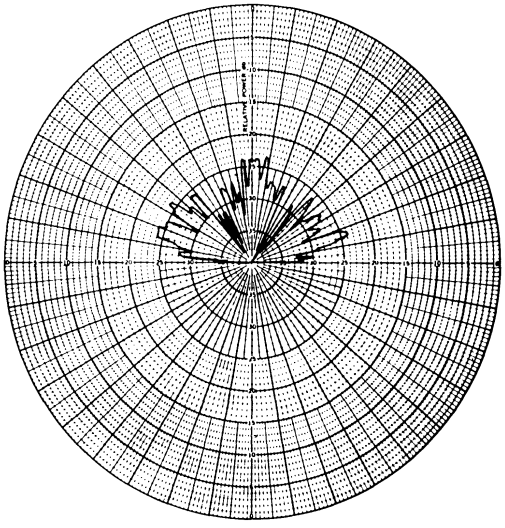

(v) f = 4.2 GHz

FIG. 5-3s-v: CROSS-POLARIZED PATTERNS OF HORN-RADANT ASSEMBLY, VHVH, 15 in. SPACING.

The transmission coefficients for the like - and cross-polarized cases are plotted in Figs. 5-4 and 5-5 for the two positions of the radant panel, at normal incidence. It is apparent that there are two ranges of frequency where the cross-polarized component is high, as predicted by the theory; one around 2.5 GHz, substantially higher in frequency than predicted, and one at 3.6 GHz as expected. Repeatability of the patterns and coefficients was about 0.7 db except at the lower resonance, where higher variations were observed. This is evidently due to the high sensitivity at resonance. Reversing the radant panel so that the horizontal dipoles face the vertically polarized transmitting horn tends to narrow the bands (see Fig. 5-5) of operation, but to give the same overall behavior. Without the dielectric sheet no differences would be expected.

It is interesting to compare Figs. 5-4 and 5-5 with Fig. 4-6, which is based on a single dipole element. The latter also shows a narrow resonance at the lower frequency band, and a broad maximum around 3.6 GHz. The effect of using a large number of elements is to reduce the bandwidth; also the gain of the radant panel would be higher at higher frequencies so that the scattered field from an array of dipoles having induced currents described by Fig. 4-6 would exhibit comparable levels of signal at the two resonant frequencies, which is the observed behavior in Figs. 5-4 and 5-5.

That the predicted and observed frequencies at the lower resonance differ is attributed to mutual coupling. Since the collecting aperture of the total radant panel of 196 elements at resonance is given by

$$A_{coll} = 196 \cdot \frac{\lambda^2 D}{2\pi} \qquad (5.1)$$

the aperture at the lower frequency is higher. In fact, the aperture predicted by Eq. (5.1) at 2 GHz is greater than the physical aperture of the radant panel. This

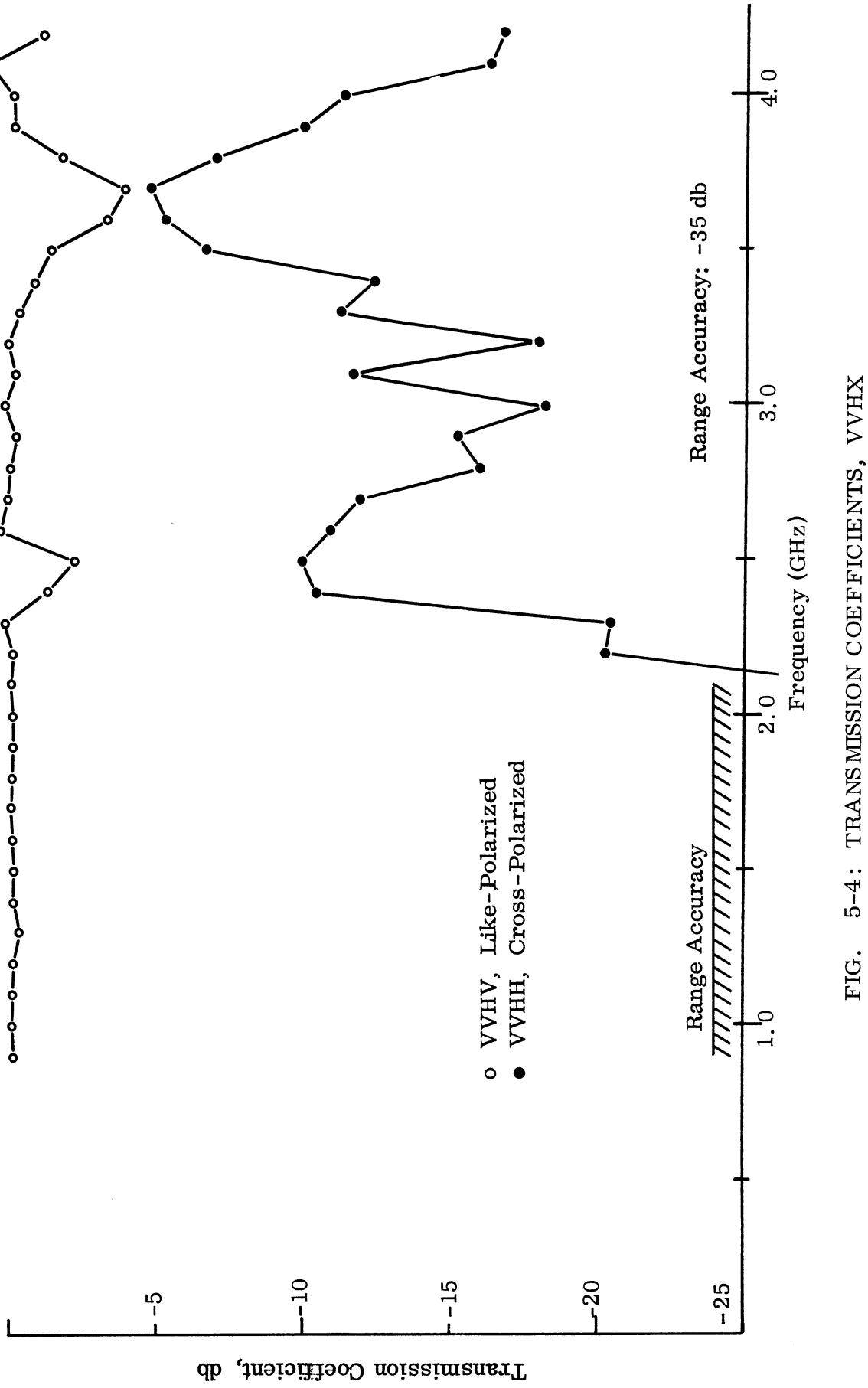

FIG. 5-4: TRANSMISSION COEFFICIENTS, VVHX

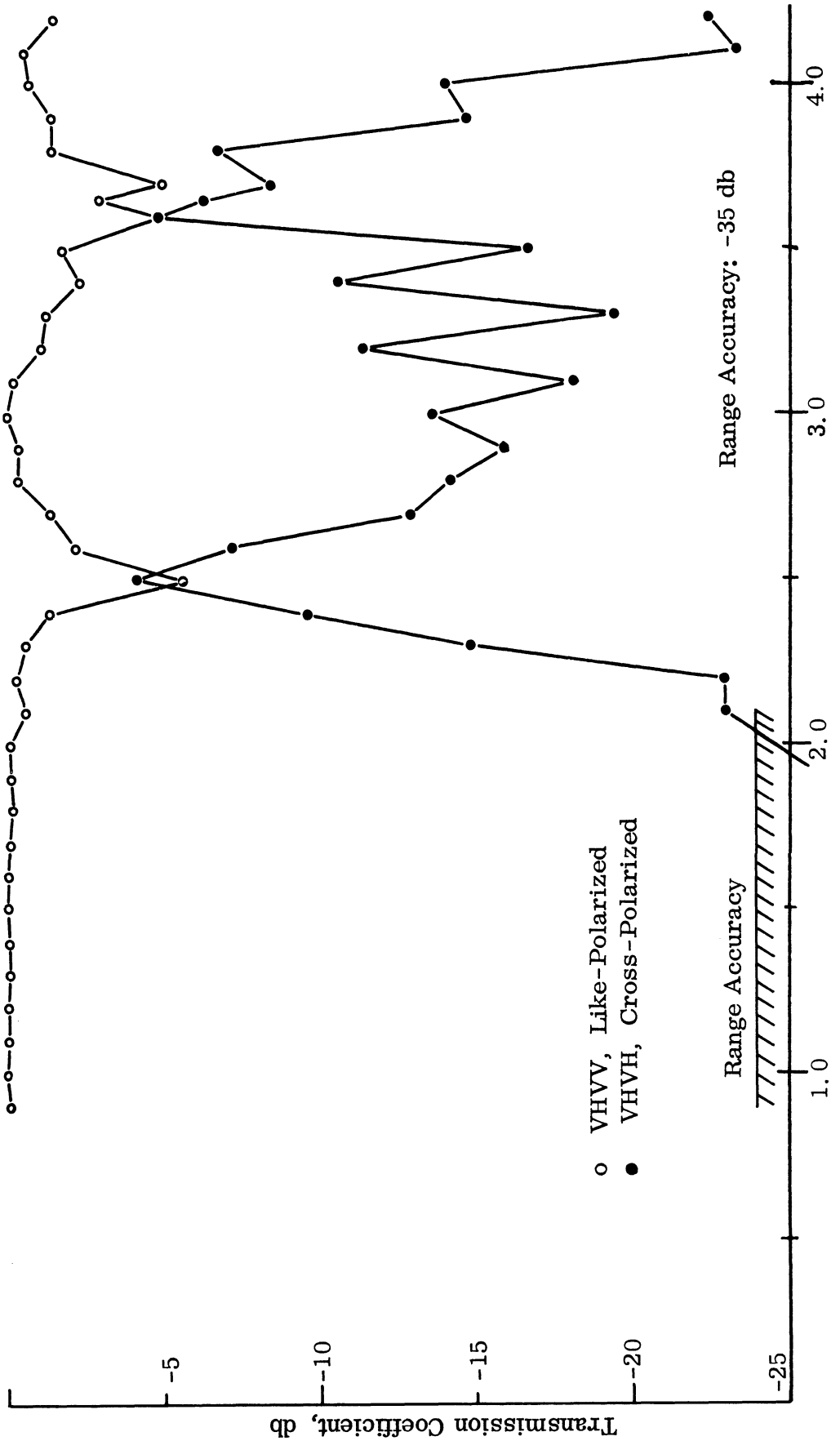

FIG. 5-5: TRANSMISSION COEFFICIENTS VHVX

would indicate a significant interference due to mutual coupling. At 3.6 GHz, the collecting aperture is substantially less than the physical aperture, and mutual coupling would not be expected to be severe.

Above 3.8 GHz, there is a deterioration of the pattern: here the interelement spacing approaches a wavelength, which implies a rising sidelobe level. This deterioration can be observed in Figs. 5-2 and 5-3 above about 3.8 GHz.

The sidelobe levels and beamwidths are plotted in Figs. 5-6 and 5-7 for the two configurations. At the higher resonance the sidelobe levels decrease to about -15 db and the beamwidths approach that of the horn. Above 3.8 GHz the sidelobe levels rise and approach the main beam level, which indicates the pattern deterioration mentioned above.

In Figs. 5-8 through 5-10 are shown some sample patterns for the incident and like-polarized cases, at frequencies near the lower resonance. The incident patterns exhibit lobes at about 75^{o} due to the rack holding the radant panel. Figure 5-8 shows the patterns at 2.3 GHz, where the effect of the radant is small. Here the shapes of the beams are similar. Approaching the resonance in Fig. 5-9 at 2.4 GHz variations are more pronounced, and at resonance in Fig. 5-10 the effect of the radant is appreciable. The level is greatly reduced, corresponding to a high conversion into the cross-polarized component. This means, too, that the scattered field of the vertical dipoles is out-of-phase with the incident field and tends to cancel it. This phenomenon is apparent also in Figs. 5-4 and 5-5.

5.2 Effects of Variation in Horn-Radant Spacing

It was observed in a prior study (Report 7300-2-T) that one effect of a panel near a horn is the change of input impedance and the increase of standing wave ratio. In addition, the sidelobe level and beam shape are affected by the spacing. Figures 5-11 and 5-12 show the patterns for both configurations at 3.6 GHz for several values of spacing. For the VVHH configuration the sidelobe level is about -16 db

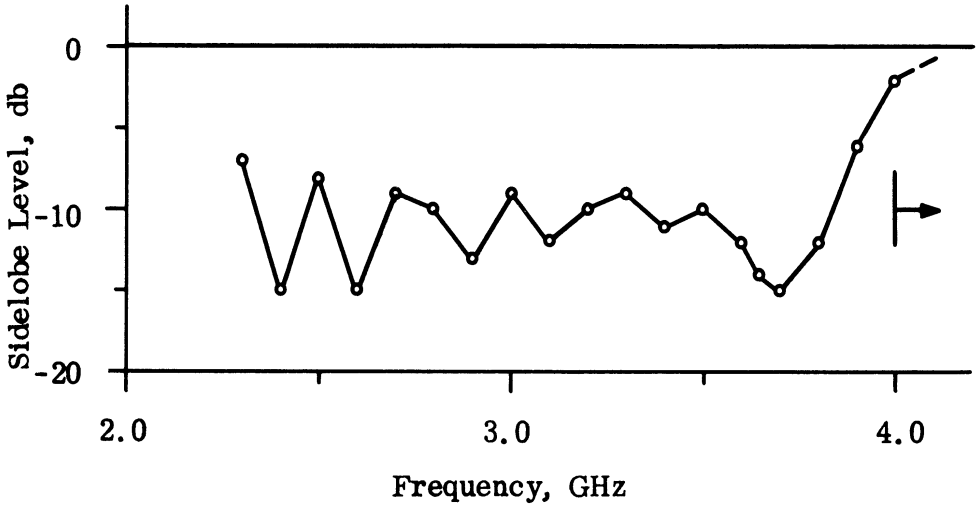

FIG. 5-6a: SIDELOBE LEVEL, VVHH

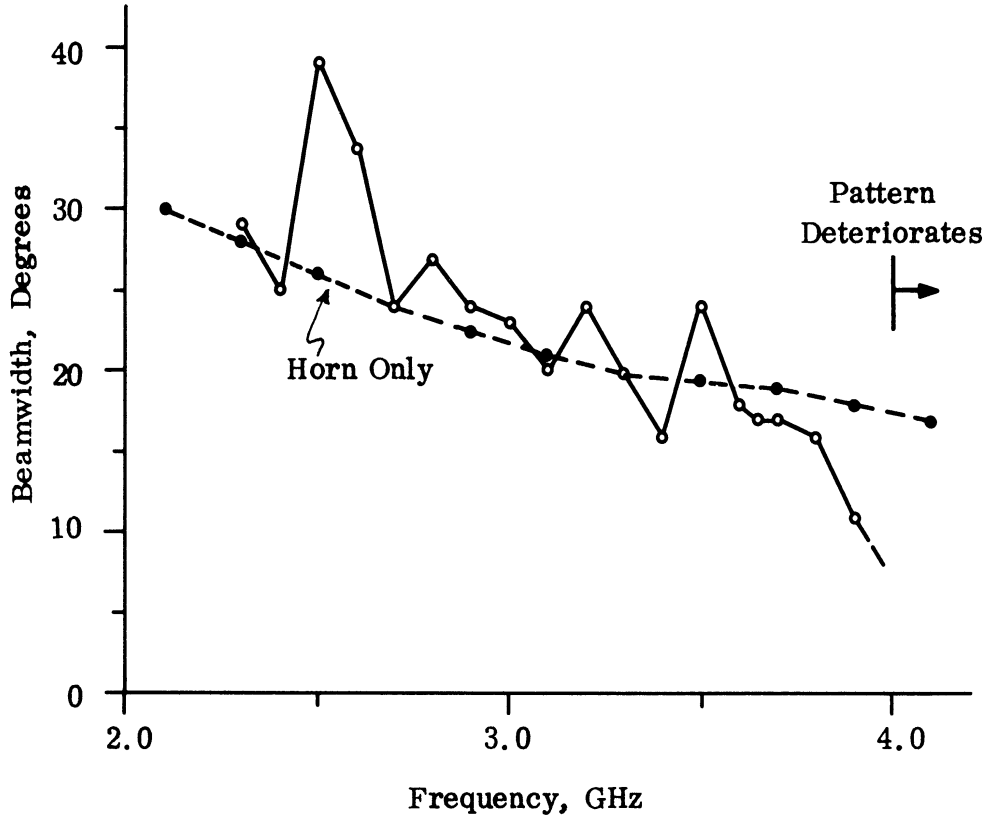

FIG. 5-6b: BEAMWIDTH, VVHH

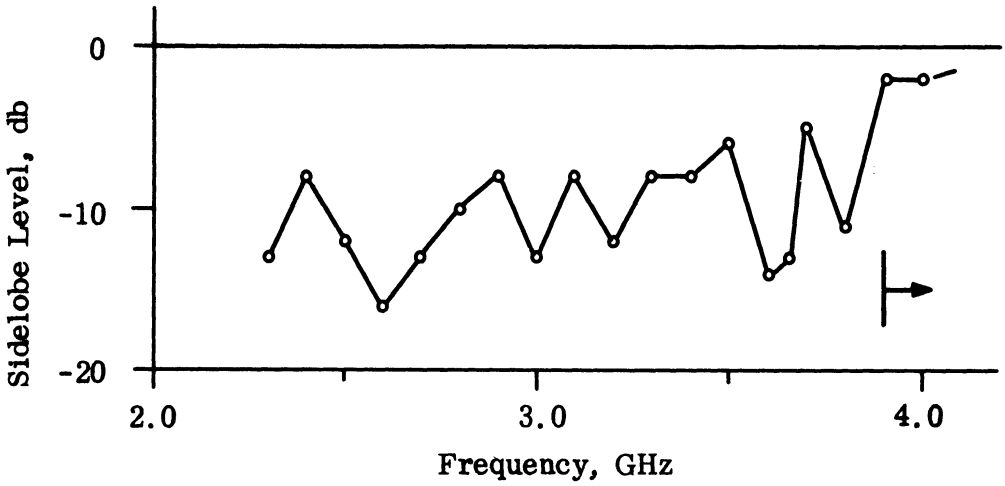

FIG. 5-7a : SIDELOBE LEVEL, VHVH

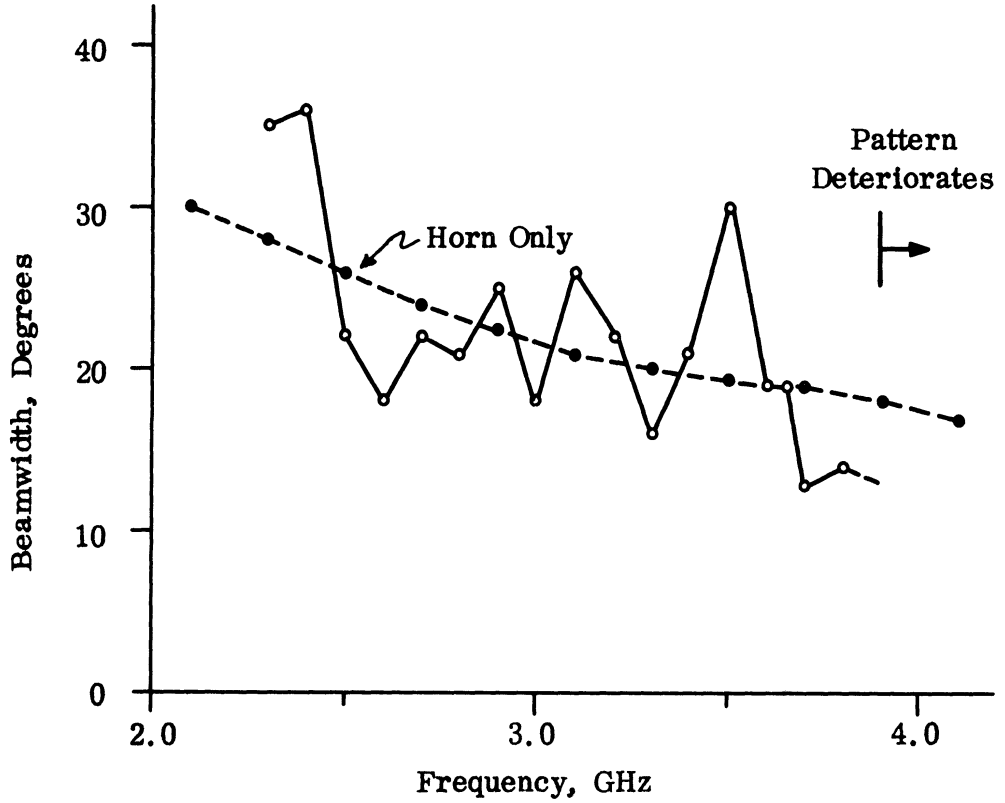

FIG. 5-7b : BEAMWIDTH, VHVH

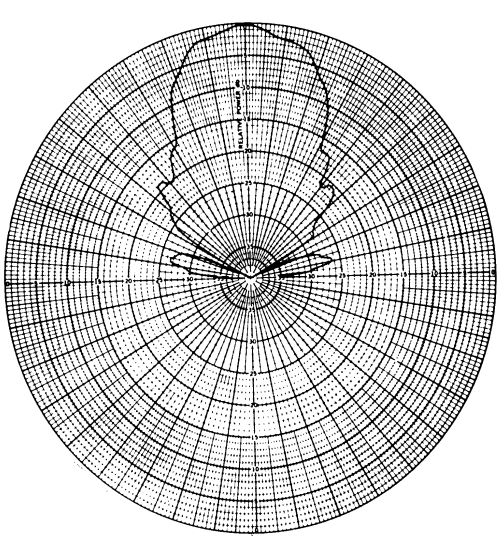

(a)

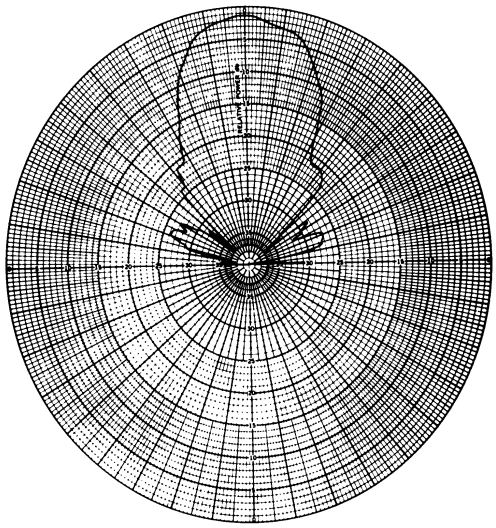

(b)

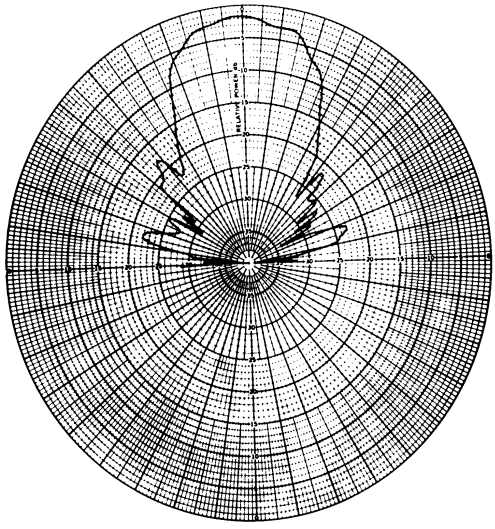

(c)

FIG. 5-8a: INCIDENT PATTERN OF HORN-RADANT ASSEMBLY AT 2.3 GHz, V--V, 15 in. SPACING.

FIG. 5-8b: LIKE-POLARIZED PATTERN OF RADANT ASSEMBLY AT 2.3 GHz, VVHV, 15 in. SPACING.

FIG. 5-8c: LIKE-POLARIZED PATTERN OF RADANT ASSEMBLY AT 2.3 GHz, VHVV, 15 in. SPACING.

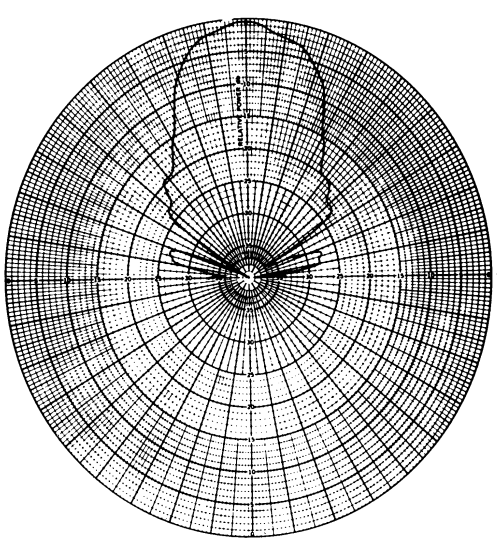

(a)

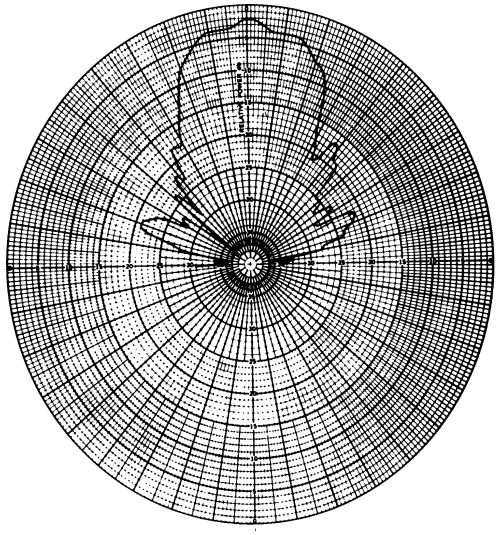

(b)

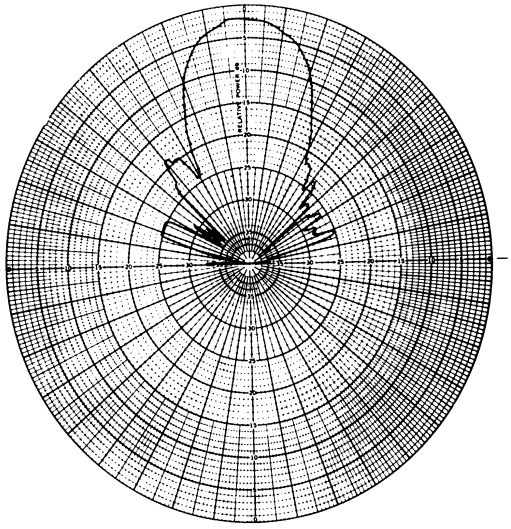

(c)

FIG. 5-9a: INCIDENT PATTERN OF HORN-RADANT ASSEMBLY AT 2.4 GHz, V--V, 15 in. SPACING.

FIG. 5-9b: LIKE-POLARIZED PATTERN OF RADANT ASSEMBLY AT 2.4 GHz, VVHV, 15 in. SPACING.

FIG. 5-9c: LIKE-POLARIZED PATTERN OF RADANT ASSEMBLY AT 2.4 GHz, VHVV, 15 in. SPACING.

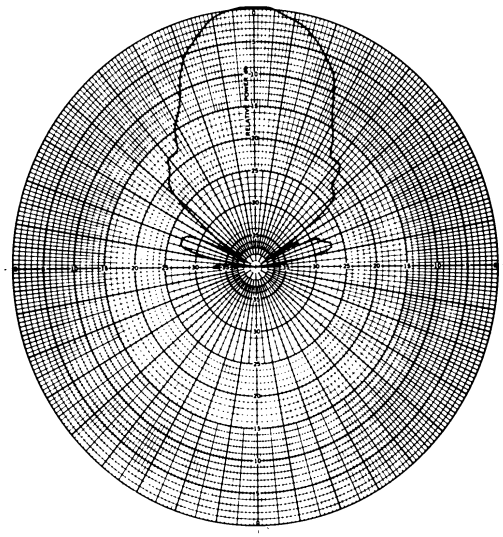

(a)

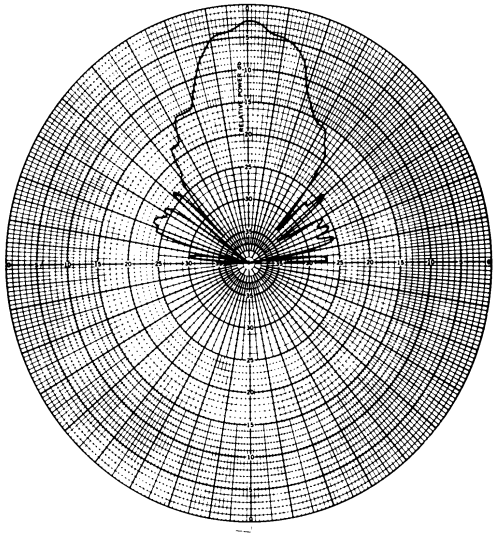

(b)

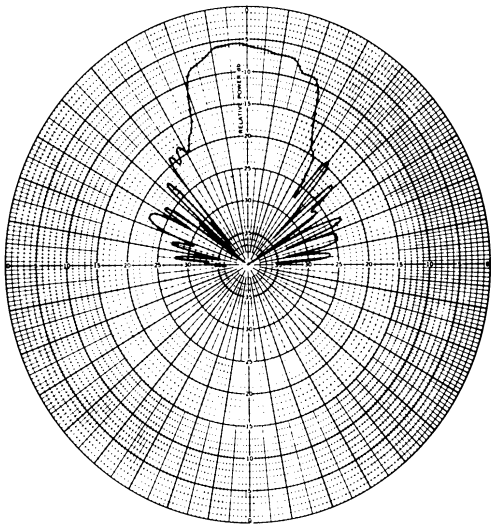

(c)

FIG. 5-10a: INCIDENT PATTERN OF HORN-RADANT ASSEMBLY AT 2.5 GHz, V--V, 15 in. SPACING.

FIG. 5-10b: LIKE-POLARIZED PATTERN OF RADANT ASSEMBLY AT 2.5 GHz, VVHV, 15 in. SPACING.

FIG. 5-10c: LIKE-POLARIZED PATTERN OF RADANT ASSEMBLY AT 2.5 GHz, VHVV, 15 in. SPACING.

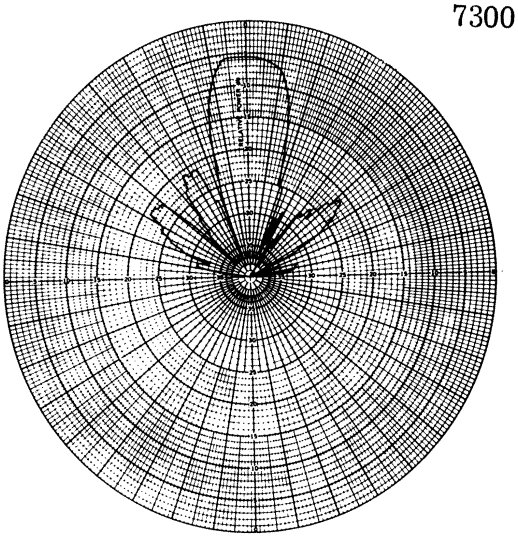

(a) 2" Spacing

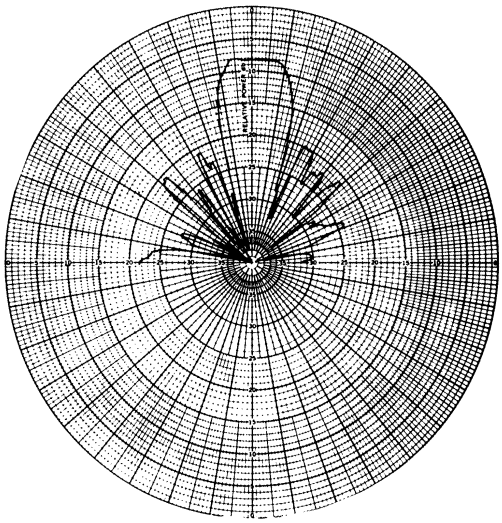

(b) 6" Spacing

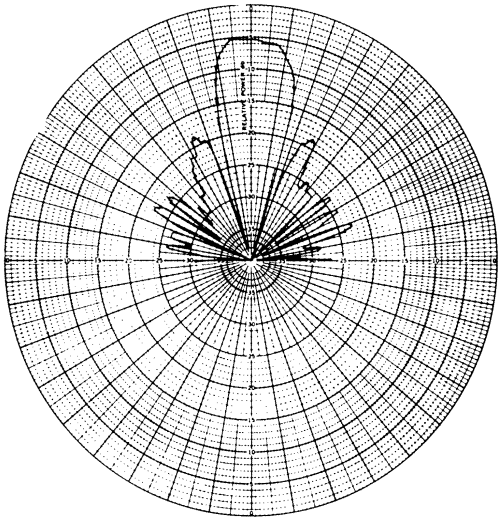

(c) 14 " Spacing

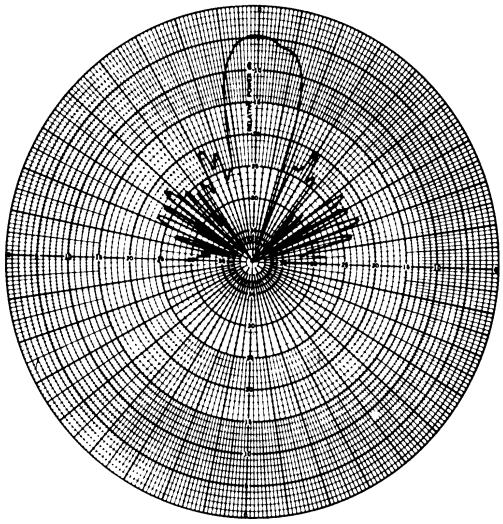

(d) 22" Spacing

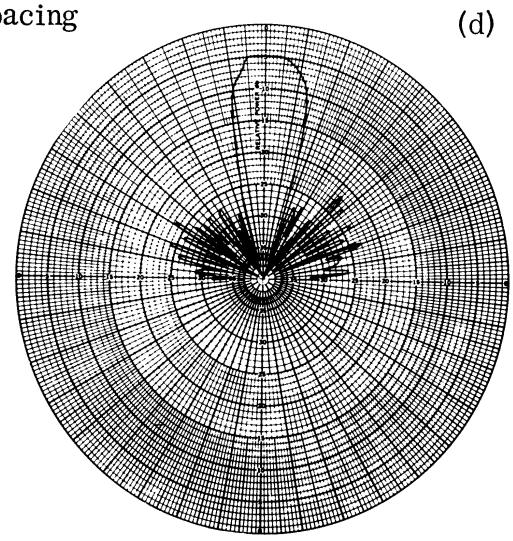

(e) 30" Spacing

FIG. 5-11a-e: CROSS-POLARIZED PATTERN, VVHH, 3.6 GHz.

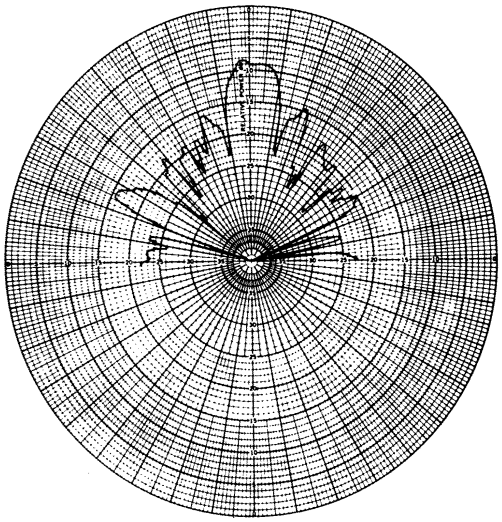

(a) 6" Spacing

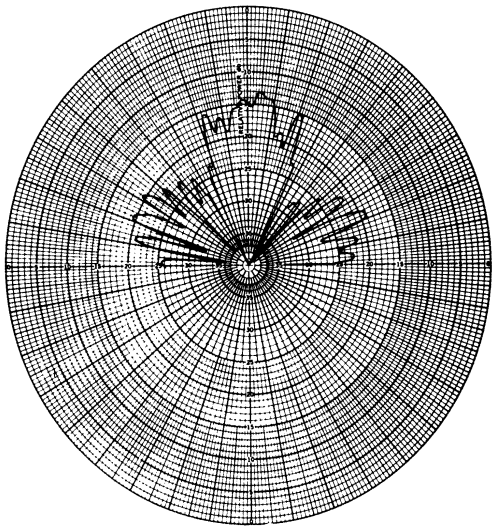

(b) 14" Spacing

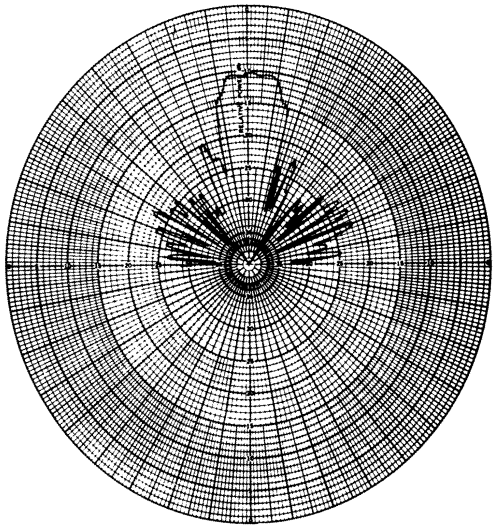

(c) 22" Spacing

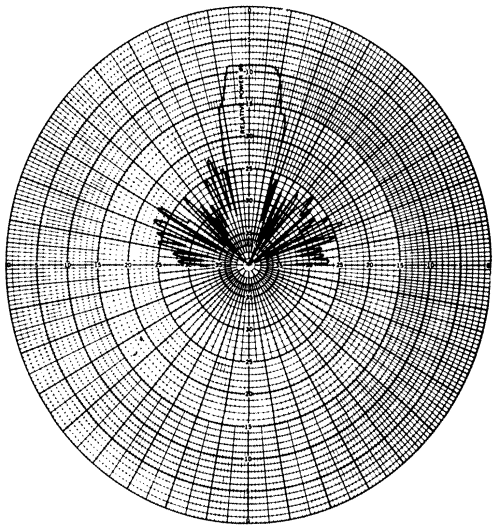

(d) 30" Spacing

FIG 5-12a-d: CROSS-POLARIZED PATTERN, VHVH, 3.6 GHz.

for all spacings, while the beam narrows slightly as spacing is increased. The VHVH configuration shows a distinct improvement at the far spacings both in sidelobe level and beam shape. This is generally true for all frequencies. The beam tends to narrow for larger spacings and sidelobe levels to decrease for both configurations. Changing the spacing shifts the resonant frequency by as much as 100 MHz for the VVHH configuration and as much as 200 MHz for the VHVH configuration.

5.3 Polarization Characteristics

In Section 3.4 it was pointed out that the scattered field of a dipole pair is in general elliptical. The relative magnitude of incident and like-polarized scattered waves is difficult to determine theoretically, owing to the complexity of the radant panel, diffraction around the panel, an unknown reflection from the panel, and interaction effects between horn and radant. Thus the polarization of the total field is better found by experiment.

Polarization patterns, obtained by rotating the transmitting horn at normal incidence, were obtained for the two configurations of the radant panel near the resonant frequencies. Both the axial ratio (ratio of major-to-minor axis) and the angle of tilt determined by the patterns are shown in Figs. 5-13 and 5-14. At the critical frequencies of 2.5 GHz and 3.7 GHz for the XVHH configuration axial ratios of less than 4 db are observed. For the XHVH configuration the upper critical frequency is 3.6 GHz with axial ratios of less than 2 db. The peaks of Figs. 5-13b and 5-14b are sharper than for the horizontal component conversion of Figs. 5-4 and 5-5. The reason for this lies in the fact that the angle of tilt of the major axis changes with frequency as well as the axial ratio; a tilting linear polarization also gives rise to a horizontal component of scattered field. Figures 5-13a and 5-14a indicate the variation of major axis inclination with frequency. Apparently near resonance the tilt angle changes abruptly from one side to the other. Sample polarization patterns are shown in Figs. 5-15a through 5-15e for the XHVH

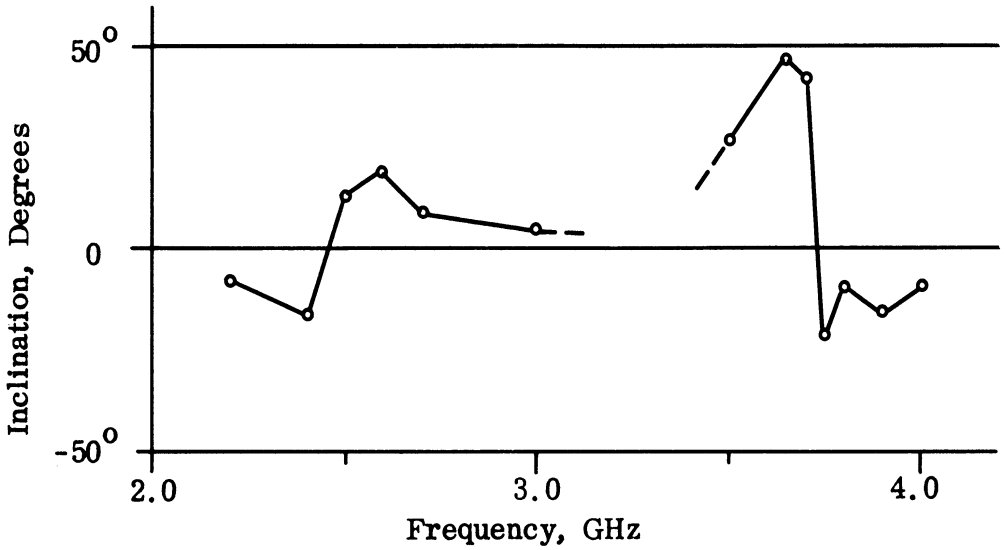

FIG.5-13a: INCLINATION OF MAJOR AXIS, XVHH

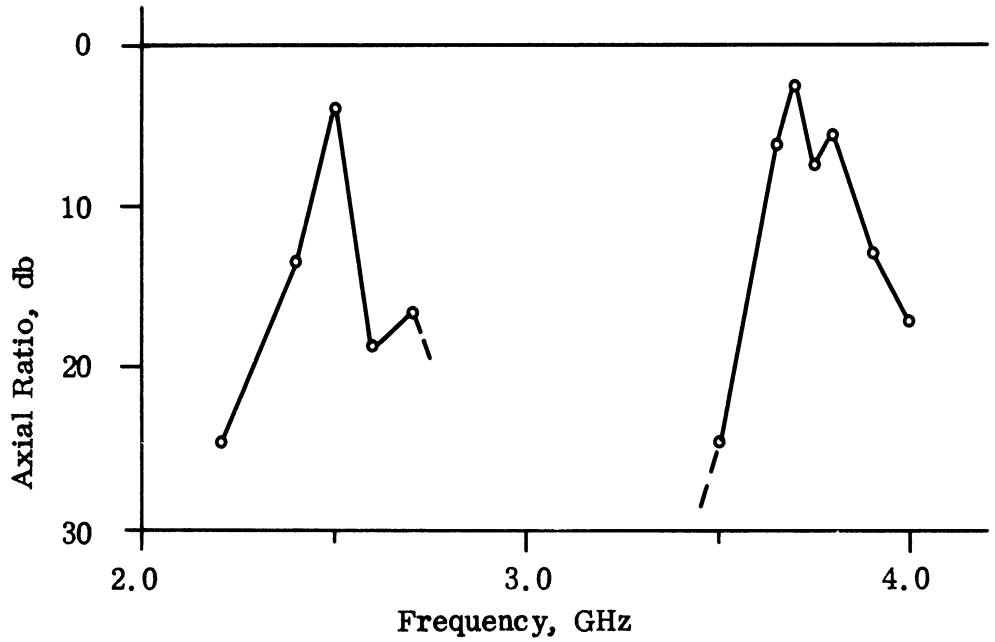

FIG.5-13b : AXIAL RATIO, XVHH

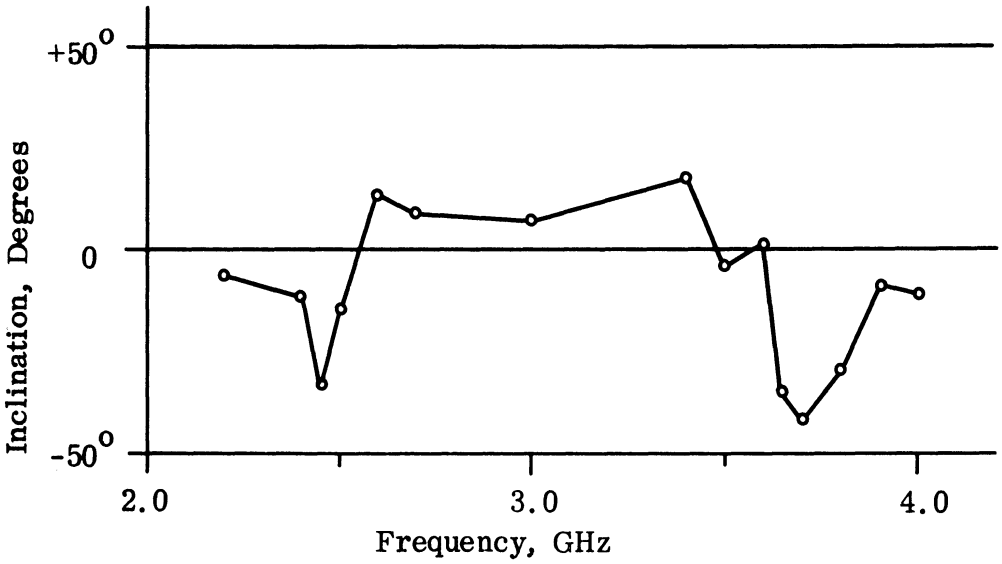

FIG. 5-14a: INCLINATION OF MAJOR AXIS, XHVH

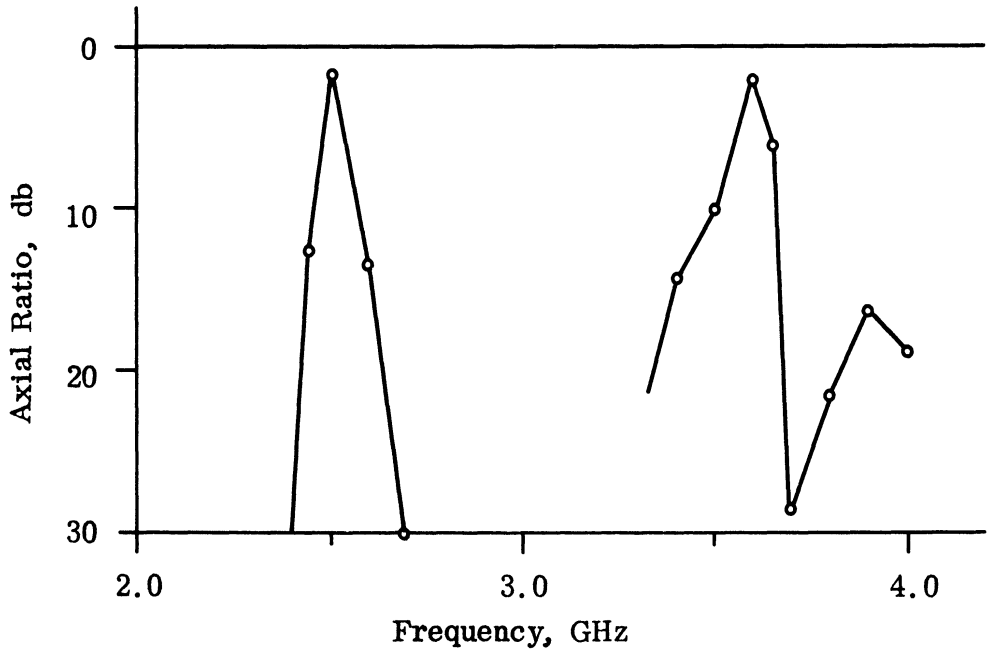

FIG. 5-14b: AXIAL RATIO, XHVH

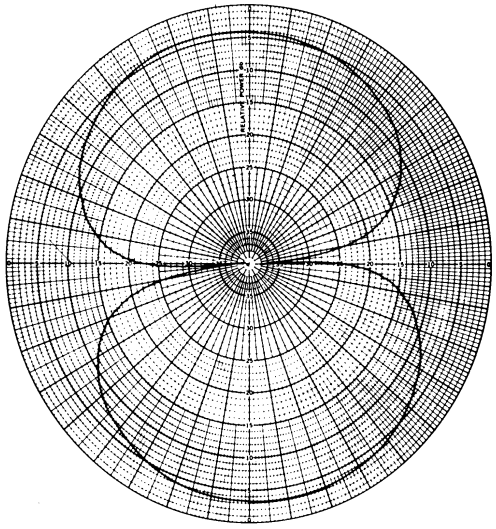

(a) f = 2.2 GHz

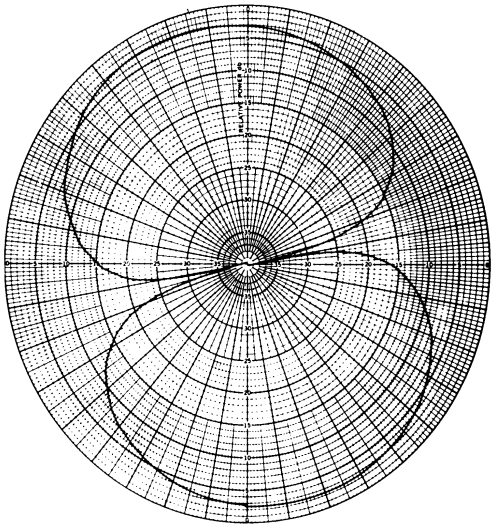

(b) f = 2.4 GHz

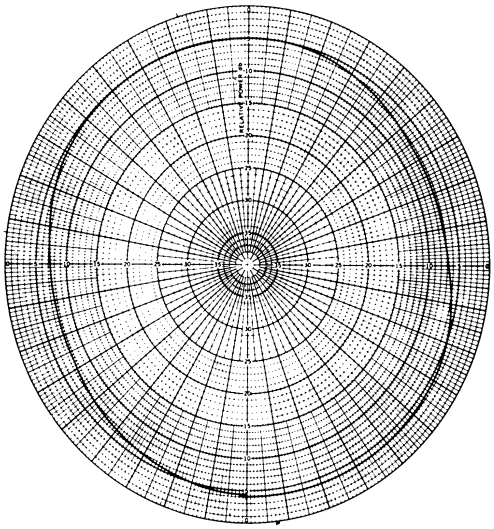

(c) f = 2.5 GHz

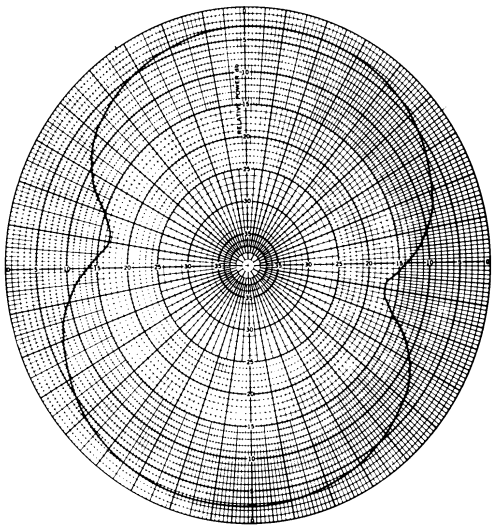

(d) f = 2.6 GHz

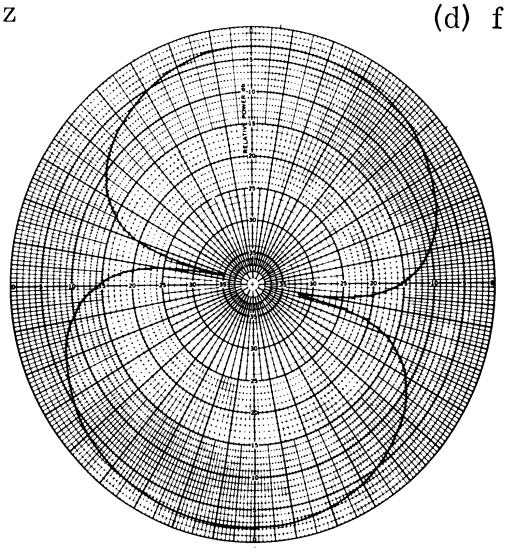

(e) f = 2.7 GHz

FIG. 5-15a-e: POLARIZATION PATTERN, XHVH, 15 in. SPACING.

configuration and demonstrate this behavior. At 2.2 GHz and 2.7 GHz the axial ratio, which is merely the ratio of the outer to inner circumscribed circles, is very small, on the order of 33 db, while the ratio of horizontal to vertical components is down only 22 db and 15 db respectively.

The patterns were repeatable within 0.3 db. The distance between antennas was 30 ft. since the 70 ft. range used for the previous data was not capable of measuring polarization patterns. This inter-antenna distance satisfies the far-field criterion for the antennas, but not for the radant. This is not expected to affect the polarization characteristics of the main beam, however.

VI

CONCLUSIONS AND RECOMMENDATIONS FOR FURTHER WORK

The results of the earlier studies indicate that the use of small loop elements close together in a dielectric panel results in a doubly anisotropic medium and provides an added degree of freedom in the design of radomes, an effect which does not appear to have been adequately exploited.

The use of the crossed-dipole sheets as a polarization converter is feasible over two narrow frequency bands. The conversion from vertical to horizontal or from vertical to circular polarization is unfortunately not as effective in terms of insertion loss and bandwidth as techniques already used (Lerner, 1965 and Kirschbaum and Chen, 1957). The effect of mutual coupling is to raise the lower resonant frequency. Due to the design chosen, the elements on each sheet are separated by more than half a wavelength above 2.5 GHz. It is felt that a higher density of dipoles would reduce see-through and improve bandwidth, but would be costly. The design would have to be based on quite different considerations than those described here, since the mutual coupling would be the dominant influence. This would then resemble the devices mentioned above, so that this does not seem a worthwhile area of further study.

Since the double anistropic panel offers the possibility of high transmission efficiency at incident angles near grazing, a further investigation of its properties and design would be desirable.

REFERENCES

King, Ronold W.P. (1956), The Theory of Linear Antennas, Cambridge, Massachusetts, Harvard University Press.

Kirschbaum, H.S. and L. Chen (July 1957), "A Method of Producing Broadband Circular Polarization Employing an Anisotropic Dielectric," IRE Trans. MTT, pp. 199-203.

Lerner, D.C. (January 1965), "A Wave Polarization Converter for Circular Polarization," IEEE Trans., AP-13, 1, pp. 3-7.

DISTRIBUTION LIST

Destination	Number of Copies
Georgia Institute of Technology Engineering Experiment Station Attn: N.E. Poulos Atlanta, Georgia 30313	1
ITT Research Institute Attn: S.L. Blum, Assistant Director Metals and Ceramics Research 10 West 35th Street Chicago, Illinois 60616	1
Illinois Institute of Technology Antenna Department 1412 Bativa, Box 205 Geneva, Illinois 60134	1
Johns Hopkins University Attn: L.B. Weckesser 8621 Georgia Avenue Silver Spring, Maryland 20910	1
Massachusetts Institute of Technology Lincoln Laboratories Attn: Document Room P.O. Box 73 Lexington,Massachusetts 02173	1
Ohio State University Research Foundation Antenna Laboratory Attn: Dr. C. Levitt 1314 Kinnear Road Columbus, Ohio 43212	1
Aeronca Manufacturing Corporation Attn: Byron Reynolds Middletown, Ohio	1

Destination	Number of Copies
Autonetics Division of North American Aviation Inc Attn: Technical Library Dept 502-41-664, Bldg 202 3370 Miraloma Avenue Anaheim, California 92680	1
Bell Aerospace Corporation Attn: Technical Library (Antenna Section) Buffalo 5, New York	1
Boeing Company Aerospace Division Attn: Robert Sutton M/F Antenna and Radome Unit P.O. Box 3707 Seattle, Washington 98124	1
Boeing Airplane Company Airplane Division Attn: C.D. Lunden P.O. Box 707 Renton, Washington 98055	1
Brunswick Corporation Attn: James Carter 325 Brunswick Lane Marion, Virginia 24354	1
Douglas Aircraft Corporation Antenna Department Attn: G.J. Cassell 3855 Lakewood Blvd Long Beach, California 90801	1
Douglas Aircraft Company, Inc Attn: Technical Library (Antenna Section) 3000 Ocean Park Blvd Santa Monica, California 90405	1

Destination	Number of Copies
Electronic Space Structures Corporation Attn: Joe Vitale Old Powder Mill Road West Concord, Massachusetts	1
Emerson and Cuming Attn: E.J. Luoma 869 Washington Street Canton, Massachusetts 02021	1
General Dynamics Attn: Robert Hallse P.O. Box 1011 Pomona, California	1
General Dynamics/Convair Attn: Gus Tricolos 3302 Pacific Coast Highway P.O. Box 1128 San Diego, California 92112	1
General Dynamics /Fort Worth Attn: J.E. Burroughs Grants Lane, P.O. Box 748 Fort Worth, Texas 76101	1
General Electric Company General Engineering Laboratory Attn: Thomas Jordan 1 River Road Schnectady, New York 12305	1
Grumman Aircraft Engineering Corporation Attn: Technical Library, M/F Avionics Bethpage, New York 11714	1
Hughes Aircraft Corporation Attn: Robert Jones Centinela and Teale Streets Culver City, California 90232	1

Destination	Number of Copies
The Martin Company Attn: Technical Library (M/F Microwave Laboratory) Box 5837 Orlando, Florida	1
The Martin Company Attn: Technical Library (Antenna Section) Baltimore, Maryland 21203	1
McDonnell Aircraft Corporation Attn: Technical Library (Antenna Section) Municipal Airport Box 516 St. Louis 66, Missouri 63166	1
Mitre Corporation Attn: Technical Library (M/F Electronic Warfare) Middlesex Turnpike P.O. Box 208 Bedford, Massachusetts 01730	1
Motorola Inc Attn: Antenna Group/Dr. Tice 8201 E McDowell Road Phoenix, Arizona 85008	1
Narmco Industries Inc Attn: Roger Long 8125 Aero Drive San Diego 11, California 92123	1
Raytheon Company Missile Systems Division Radome Section Attn: Robert O. Howe Bedford, Massachusetts 01730	1

Destination	Number of Copies
Technical Research Group Attn: Librarian Antenna Section 130 Constitution Drive Menlo Park, California	1
Director AUL (31-AVE-51-30) Maxwell AFB Alabama 36112	1
DDC Cameron Station Alexandria, Virginia 22314	20 + card
AFAL (AVWE-3) Wright-Patterson AFB Ohio 45433	75
SEG (SEACA/Mr. George F. Duree) Wright-Patterson AFB Ohio 45433	1
AFAL (AVNT) Wright-Patterson AFB Ohio 45433	1
AFCRL (CRRD) L.G. Hanscom Field Bedford, Massachusetts 01730	1
APGC (PGVEP-3) Eglin AFB Florida 32542	1
AFMTC (Technical Library) Patrick AFB Florida 32925	1
AFMDC (Technical Library) Holloman AFB New Mexico 88330	1
Central Intelligence Agency Code SAN 2430 E St SW Washington DC 20505	1
Director Ballistics Research Laboratory Attn: Ballistics Measurement Laboratory Aberdeen Proving Ground, Maryland 21005	1

Destination	Number of Copies
Commander US Army White Sands Signal Agency Attn: SIGWS-FC-02 White Sands, New Mexico 88002	1
US Naval Ordnance Laboratory Attn: Paul Fisher Attn: Code LX/G. N. Plotkin White Oak Silver Springs, Maryland	1
US Naval Research Laboratory Attn: Dr. A.E. Marston Code 5250 Washington DC 20390	1
National Bureau of Standards Department of Commerce Attn: Dr. A.G. McNish Washington DC	1
Chief, Technical Library Office of Assistant Secretary of Defense (R and D) Room 3E1065 Washington DC 20330	1
Scientific and Technical Information Facility Attn: NASA Representative (SAK/DL) P.O. Box 5700 College Park, Maryland 20740	1
Chief, Bureau of Naval Weapons Attn: RRMA-31/Charles Bersch Washington DC 20370	1
AFWL (WLRJ/Mr. W.J. Moulds) Kirtland AFB New Mexico 87117	1
Commander AF Office of Scientific Research Attn: SREC Washington DC	1

Destination	Number of Copies
NADC Attn: George Tatnell Johnsville, Pennsylvania 18974	1
RTD (RTTH) Bolling AFB DC 20332	1
	145

UNCLASSIFIED

Security Classification

DOCUMENT CONTROL DATA - R&D

(Security classification of title, body of abstract and indexing annotation must be entered when the overall report is classified)

1. ORIGINATING ACTIVITY *(Corporate author)*
The University of Michigan Radiation Laboratory
Department of Electrical Engineering
Ann Arbor, Michigan 48108

2a. REPORT SECURITY CLASSIFICATION
UNCLASSIFIED

2b. GROUP

3. REPORT TITLE

Radant Analysis Studies

4. DESCRIPTIVE NOTES *(Type of report and inclusive dates)*
Final Report-Phase II-- 1 March 1966 through 1 January 1967

5. AUTHOR(S) *(Last name, first name, initial)*

Tai, Chen-To, and Kalafus, Rudolph M.

6. REPORT DATE	7a. TOTAL NO. OF PAGES	7b. NO. OF REFS
February 1967	60	3

8a. CONTRACT OR GRANT NO.	9a. ORIGINATOR'S REPORT NUMBER(S)
AF 33(615)-2811	7300-2-F
b. PROJECT NO 4161	
c. 416103	9b. OTHER REPORT NO(S) *(Any other numbers that may be assigned this report)*
d.	AFAL-TR-67-62

10. AVAILABILITY/LIMITATION NOTICES This document is subject to special export controls and each transmittal to foreign governments or foreign nationals may be made only with prior approval of AFAL (AVWE-3), Wright -Patterson AFB Ohio 45433.

11. SUPPLEMENTARY NOTES	12. SPONSORING MILITARY ACTIVITY
	Air Force Avionics Laboratory, AVWE Research and Technology Division Air Force Systems Command Wright-Patterson AFB, Ohio 45433

13. ABSTRACT

A review is given of the work performed on the loop-loaded radant panel, and its transmission properties. The recent work covered in detail herein deals with the transmission and polarization transformation properties of the crossed-dipole radant panel. A theoretical treatment is given based on knowledge of the element input impedance. The experimental program is described which yields information on transmission properties, polarization characteristics, beamwidth, bandwidth, sidelobe level, and patterns.

DD FORM 1 JAN 64 1473

UNCLASSIFIED

Security Classification

14. KEY WORDS	LINK A		LINK B		LINK C	
	ROLE	WT	ROLE	WT	ROLE	WT
Wave Polarization Converter Radant Experimental Study						

INSTRUCTIONS

1. ORIGINATING ACTIVITY: Enter the name and address of the contractor, subcontractor, grantee, Department of Defense activity or other organization *(corporate author)* issuing the report.

2*a*. REPORT SECURITY CLASSIFICATION: Enter the overall security classification of the report. Indicate whether "Restricted Data" is included. Marking is to be in accordance with appropriate security regulations.

2*b*. GROUP: Automatic downgrading is specified in DoD Directive 5200.10 and Armed Forces Industrial Manual. Enter the group number. Also, when applicable, show that optional markings have been used for Group 3 and Group 4 as authorized.

3. REPORT TITLE: Enter the complete report title in all capital letters. Titles in all cases should be unclassified. If a meaningful title cannot be selected without classification, show title classification in all capitals in parenthesis immediately following the title.

4. DESCRIPTIVE NOTES: If appropriate, enter the type of report, e.g., interim, progress, summary, annual, or final. Give the inclusive dates when a specific reporting period is covered.

5. AUTHOR(S): Enter the name(s) of author(s) as shown on or in the report. Enter last name, first name, middle initial. If military, show rank and branch of service. The name of the principal author is an absolute minimum requirement.

6. REPORT DATE: Enter the date of the report as day, month, year; or month, year. If more than one date appears on the report, use date of publication.

7*a*. TOTAL NUMBER OF PAGES: The total page count should follow normal pagination procedures, i.e., enter the number of pages containing information.

7*b*. NUMBER OF REFERENCES: Enter the total number of references cited in the report.

8*a*. CONTRACT OR GRANT NUMBER: If appropriate, enter the applicable number of the contract or grant under which the report was written.

8*b*, 8*c*, & 8*d*. PROJECT NUMBER: Enter the appropriate military department identification, such as project number, subproject number, system numbers, task number, etc.

9*a*. ORIGINATOR'S REPORT NUMBER(S): Enter the official report number by which the document will be identified and controlled by the originating activity. This number must be unique to this report.

9*b*. OTHER REPORT NUMBER(S): If the report has been assigned any other report numbers *(either by the originator or by the sponsor)*, also enter this number(s).

10. AVAILABILITY/LIMITATION NOTICES: Enter any limitations on further dissemination of the report, other than those imposed by security classification, using standard statements such as:

(1) "Qualified requesters may obtain copies of this report from DDC."

(2) "Foreign announcement and dissemination of this report by DDC is not authorized."

(3) "U. S. Government agencies may obtain copies of this report directly from DDC. Other qualified DDC users shall request through

_____."

(4) "U. S. military agencies may obtain copies of this report directly from DDC. Other qualified users shall request through

_____."

(5) "All distribution of this report is controlled. Qualified DDC users shall request through

_____."

If the report has been furnished to the Office of Technical Services, Department of Commerce, for sale to the public, indicate this fact and enter the price, if known.

11. SUPPLEMENTARY NOTES: Use for additional explanatory notes.

12. SPONSORING MILITARY ACTIVITY: Enter the name of the departmental project office or laboratory sponsoring *(paying for)* the research and development. Include address.

13. ABSTRACT: Enter an abstract giving a brief and factual summary of the document indicative of the report, even though it may also appear elsewhere in the body of the technical report. If additional space is required, a continuation sheet shall be attached.

It is highly desirable that the abstract of classified reports be unclassified. Each paragraph of the abstract shall end with an indication of the military security classification of the information in the paragraph, represented as *(TS), (S), (C), or (U)*.

There is no limitation on the length of the abstract. However, the suggested length is from 150 to 225 words.

14. KEY WORDS: Key words are technically meaningful terms or short phrases that characterize a report and may be used as index entries for cataloging the report. Key words must be selected so that no security classification is required. Identifiers, such as equipment model designation, trade name, military project code name, geographic location, may be used as key words but will be followed by an indication of technical context. The assignment of links, rules, and weights is optional.